Fall 2016

Eis analysis of shear enhanced microfluidic lab-on-a-chip device

Mehnaz Mursalat
New Jersey Institute of Technology

Copyright Warning & Restrictions

The copyright law of the United States (Title 17, United States Code) governs the making of photocopies or other reproductions of copyrighted material.

Under certain conditions specified in the law, libraries and archives are authorized to furnish a photocopy or other reproduction. One of these specified conditions is that the photocopy or reproduction is not to be "used for any purpose other than private study, scholarship, or research." If a, user makes a request for, or later uses, a photocopy or reproduction for purposes in excess of "fair use" that user may be liable for copyright infringement,

This institution reserves the right to refuse to accept a copying order if, in its judgment, fulfillment of the order would involve violation of copyright law.

Please Note: The author retains the copyright while the New Jersey Institute of Technology reserves the right to distribute this thesis or dissertation

Printing note: If you do not wish to print this page, then select "Pages from: first page # to: last page #" on the print dialog screen

ABSTRACT

EIS ANALYSIS OF SHEAR ENHANCED MICROFLUIDIC LAB-ON-A-CHIP DEVICE

by
Mehnaz Mursalat

Electrochemical sensors and biosensors have received much attention owing to the feasibility demonstrated regarding instrumental simplicity, decent cost, and portability during the detection of a wide range of biological and pharmaceutical macromolecules. Carbon-based nanomaterials, including carbon nanotubes, have garnered tremendous interest for their unique thermal, mechanical, electronic and catalytic properties while designing these sensors. Whenever the macromolecules interact with a bio-recognition element on the electrode transducer surface, a measurable change in the electrical current or potential takes place. To achieve lower limits of detection, the use of sensor surfaces modified with nanostructured materials such as nanotubes, or nanoparticles is becoming increasingly significant. The study aims to design a CNT-based electrochemical glass sensor which purifies monoclonal antibody in the presence of its biorecognition element (e.g. an antigen). The system utilizes an open-flow carbon nanotube platform for monoclonal antibody purification using impedance-based sensing (EIS). The open flow allows rapid concentration of the target molecules and shear-enhanced specificity leading to maximum hydrodynamic shear force. Interdigitated electrodes are used to trap multi-walled carbon nanotubes. The principals involved in fabricating such a device can be applied for the detection of some other pharmaceutical molecules. At the same time, CNTs replaced by ZnO and Al_2O_3 based nanomaterials can also be taken into account for detection of various macromolecules for better sensitivity and better specificity.

EIS ANALYSIS OF SHEAR ENHANCED MICROFLUIDIC LAB-ON-A-CHIP DEVICE

by
Mehnaz Mursalat

A Thesis
Submitted to the Faculty of
New Jersey Institute of Technology
in Partial Fulfillment of the Requirements of the Degree of
Master of Science in Chemical Engineering

Department of Chemical, Biological and Pharmaceutical Engineering

January 2017

APPROVAL PAGE

REAL TIME, INTEGRATED, PAPER BASED TEMPERATURE SENSOR FOR LAB ON A CHIP DEVICE

Vignesh Shekhar

Dr. Sagnik Basuray, Thesis Advisor — Date
Assistant Professor of Chemical Engineering, NJIT

Dr. Robert B. Barat, Committee Member — Date
Professor of Chemical Engineering, NJIT

Dr. Laurent Simon, Committee Member — Date
Associate Professor of Chemical Engineering, NJIT

Dr. Dong Kyun Ko, Committee Member — Date
Assistant Professor of Electrical and Computer Engineering, NJIT

BIOGRAPHICAL SKETCH

Author: Mehnaz Mursalat

Degree: Master of Science

Date: January 2017

Undergraduate and Graduate Education:

- Master of Science in Chemical Engineering,
  New Jersey Institute of Technology, New Jersey, 2017

- Bachelor of Science in Chemical Engineering,
  Bangladesh University of Engineering and Technology, Dhaka, 2014

Major: Chemical Engineering

This Thesis is dedicated to all of my loved ones;
my Parents, Grandparents, Family and Friends

ACKNOWLEDGMENT

I would like to take this opportunity to thank the Almighty and all the people who have been instrumental in making me who I am today. Here are some wonderful people without whose help, this project would not have been possible.

It is with great admiration and respect that I acknowledge the support of Dr. Sagnik Basuray, who is my thesis advisor, throughout my graduate study. I would like to thank him for taking an active interest in all the details of my work and for guiding me all the way through.

My deepest appreciation and acknowledgment goes to my committee members, Dr. Kamalesh Sirkar and Dr. Somenath Mitra. I thank both for being ever so approachable and helpful.

I would like to thank my fellow lab mates Nida, Mengxin, Natalija, Bhuvana, Andrew, Victoria, Nikki and Vignesh for their help and guidance through my research.

Last but not the least, all of this would be for naught unless the support and love of my parents, grandparents, family members, teachers, and friends were there.

TABLE OF CONTENTS

Chapter **Page**

TABLE OF CONTENTS (Continued)

Chapter **Page**

LIST OF TABLES

LIST OF FIGURES

LIST OF FIGURES (Continued)

LIST OF FIGURES (Continued)

CHAPTER 1

INTRODUCTION

Microfluidics involves the control and manipulation of fluids ranging from microliters (10^{-6}) to picoliters (10^{-12}) in an array of channels with dimensions as low as tens to hundreds of microns [1]. These devices exhibit excellent analytical performance in sensing biomolecules without consuming high energy while minimizing dead volume, void volume or sample carry over [2]. The high surface to volume ratio contributes to increased reactions [2]. They also have inherent advantages like a decrease in sample and reagent consumption leading to significant reductions in operational cost [3]. Further, the microfluidic devices are portable, reliable and multi-functional. Hence, microfluidic devices are indeed being explored across a vast plethora of applications from sensing to nanoscale purification [3]. Glass has been the material of choice in constructing microfluidic device owing to its superior thermal conductivity, surface stability, and solvent compatibility [4]. Further glass has high optical transparency, well-defined surface chemistries, and excellent high-pressure resistance make it a substrate of preference for many microfluidic and non-microfluidic applications [5]. Glass is also biocompatible, chemically inert, and hydrophilic and allows efficient coatings [5].

The use of microelectrodes is prevalent in microfluidic devices. Microelectrodes are three-dimensional electrodes that have excellent sensitivity for electro-analysis [6]. The three-dimensional architecture of the microelectrodes leads to increased penetration of the electric lines of forces into the bulk, while the nano-ordered texture results in increased surface area [6]. This increase in size facilitates electron transfer rates and creates more

sites for the attachment of molecular probes [6]. Microelectrodes have been used for the rapid detection of nucleic acids in aM and pM concentrations [7]. Microelectrodes are ideal for samples where low volumes are desired owing to their small dimensions [7, 8]. By reducing down, the dimensions of the electrode and the electrochemical cell, an increase in the diffusional flux to the electrode surface can be achieved [8]. Another major advantage that microelectrodes introduce is the decrease in noise and a concomitant increase in signal to noise ratio [9].

In microfluidics, Electronic Impedance Spectroscopy (EIS) based sensing has proven to be an efficient method for biomolecule characterization [10]. It is a nondestructive technique used for the analysis of charge transport owing to chemical diffusion, adsorption or desorption in a system [11]. EIS appears to be an extensively applied tool in corrosion and battery studies where changes in surface properties of materials take place as a result of variations in surface chemical composition [12, 13]. For the analysis of biomolecules, many of the existing methods require them to be modified with fluorescence dyes, enzymes, redox or radioactive labels whereas EIS incorporates a label-free nondestructive detection methodology [11, 14]. Further, EIS ensures accuracy and repeatability in measurements, thus its superiority over other existing voltammetry/amperometry methods such as cyclic voltammetry and potential coulometry used for the characterization or sensing of biomolecules [15]. Cyclic voltammetry requires analyte concentrations of 10^{-3} to 10^{-5} M while EIS achieves a significantly lower detection limit in the nanomolar region [16]. The same goes with potential coulometry whose detection limit ranges in the molar region [17].

In EIS, electrochemical impedance is usually measured by applying an AC potential across an electrochemical cell [18]. This small amplitude sinusoidal voltage signal results in a measurable current response[18]. The electrochemical changes occurring at electrodes are translated as either resistive or capacitive property change of materials. This change is called a change of impedance. The obtained EIS data is commonly analyzed by fitting it to an equivalent electrical circuit model that consists of common electrical components such as resistors, capacitors, and inductors [19]. For example, any electrolytic reactions at the electrode are modeled as a charge transfer resistance coupled with a constant potential element. The Debye double layer that forms at the electrodes is modelled as a capacitor. The EIS models and their physical interpretation is described in details in Chapter 3 [19].One of the major reasons for choosing carbon nanotubes (CNT) in this work is CNT's advantageous chemical, mechanical, thermal and electrical properties. These properties include high electrical conductivity, high tensile Strength and flexibility and low Thermal Expansion Coefficient [21].

Carbon Nanomaterial-based electrochemical sensors have been used for detection of various analytes such as antibodies, antigens, proteins and DNA [20]. Carbon possesses the capacity to hybridize into sp, sp2 configurations with narrow gaps between their 2s and 2p electron shells [21]. It has been found that this simple hybrid structure can facilitate the sensitive detection of the biomolecule. Provided if on the interaction of the biomolecule with carbon material specifically at the sp, sp^2 hybridization, a π electron orbital is formed [21]. This π electron increases the conductivity which is a quantitative and qualitative measure of the biomolecular interaction [20]. Existing antibody detection method include enzyme-linked immunosorbent assay (ELISA), radioimmunoassay, and electrophoretic

immunoassay. However, these techniques involving e extensive sophisticated instrumentation is complex and require expensive reagents [22]. Therefore there is a critical necessity to develop cost-effective Lab-on-a-chip microfluidic devices with enhanced sensitivity, reliability, repeatability and low detection limit that incorporate EIS as the detection methodology. [23]

An active research area is a study of monoclonal antibodies (mAbs) [24]. The increasing demand of mAbs and polyclonal antibodies (pAbs) is fueled by their promise to treat multiple diseases including cancer, rheumatoid arthritis, and cardiovascular disease [25]. Hence, there is an increasing demand for a large number of highly specific and sensitive mAbs for research, clinical and therapeutic use. mAbs effectiveness as a therapeutic agent is high if they demonstrate a long serum half-life, low immunogenicity, a high affinity for the antigen, and can neutralize the activity of the antigen. In fact, over the past decade, a high demand of high purity mAbs has been observed for the purpose of direct labeling by biomarkers [24, 25]. For mAb extraction, cell lines are created by fusing a mouse myeloma with mouse spleen cells from an immunized donor [26]. The mAbs are then expressed by this cells. Cell lysis is done and the cell culture fluid (CCF) (contains the lysis contents of the cells) collected. Any mAb purification methodology from the CCF has to prevent contamination from foreign proteins (such as insulin or transferrin) [27]. These contaminants can mimic the binding of the mAbs to the cells upon binding to the specific membrane-bound receptors [27]. Thus, the presence of this foreign proteins restricts the use of insufficiently purified mAbs for any biological testing system as any adverse effect might be falsely attributed to the mAbs [28]. The purification process for mAb needs to reliably and predictably produce a product suitable for human use. Impurities

such as host cell protein, endogenous viruses, DNA and endotoxin, aggregates and other species demand removal while maintaining an acceptable yield [20]. Further, impurities introduced during the purification process has to be removed. The impurities include leached Protein A, extractable from resins and filters and so on [24, 29]. Thus, mAbs purification strategies require high purity of mAbs with no contaminants.

The existing methods to purify mAbs include Gas Chromatography (GC) and High-pressure liquid chromatography (HPLC) [30]. However, these methods are cumbersome and often fail to achieve the desired level of purification. Further these methods require extensive instrumentation with large expenses. However, microfluidics can be a serious alternative that offers the advantages of low sample consumption, is cost-effective, simple and can be easily packaged into a small device [31] [32].

To avoid the problems in mAbs purification, a microfluidic platform is envisioned that uses shear force to achieve effective purification. Further, this platform will allow affinity testing and for testing the efficacy of mAbs. The platform is adapted from an earlier work by Dr. Basuray that has interdigitated electrodes, and a microchannel packed with carbon nanotubes (CNTs) functionalized with an oligo (a short single-stranded DNA (ssDNA)) [5, 6]. A solution compromised of target ssDNA (ssDNA complementary to the oligo) and other ssDNA flows through the platform [33]. At a given solution velocity the target ssDNA remains hybridized to the oligo while any non-target ssDNA is sheared off the oligo; breaking the hydrogen bonds. Thus, it can be hypothesized that the shear forces in the microchannel are close to the hydrogen bond strength at some flow rate. It is well documented that a mAb-antigen pair has a significantly weaker binding force in comparison to the hydrogen bond of the DNA [34]. Thus the shear-enhanced flow at

different flow rates can specifically bind mAb to antigen and can also shear mAbs from the antigen. This binding and stripping event of the mAbs to the CNT-mAbs complex triggers changes in the observed EIS signal observed. Thus, EIS can be used to interpret the binding strength and structural changes of the mAbs [35].

To interpret the EIS results, the physics of the interactions of the CNT-Protein A-mAb complex has to be represented as an equivalent circuit. It is hypothesized that the EIS signal is generated from local domain perturbations at the CNT interface. These domains are ~ nM due to the nanostructured CNT packing in the channel [36]. Thus EIS needed to be modeled in nano-domains to interpret it as equivalent circuits to describe the experimental details. These allows to develop correlations linking the equivalent circuit elements of physical processes and ultimately, linking antibody structure dynamics to EIS perturbations or signature [36]. Correlations also need to be developed for changes in EIS due to a perturbation in pH, ionic strength and flow rates (shear). The study here looks at the critical questions. Namely, how shear force can degrade the efficiency and affinity of the mAb specifically in physiologically relevant solutions and how pH and ionic strength in conjugation with shear, affect mAb efficiency and affinity.

In this study, a simple monoclonal-polyclonal antibody attachment was analyzed for the ease of modeling an equivalent circuit. The selection of this simple system stems from the need of modeling an even more complex system that involves the binding of a mAb to Protein A. Further; it is shown how this study can be used to develop biosensors with high sensitivity for antibody detection. As this device is based on the electrical response of functionalized CNT to antibody binding, they can be easily turned to detect other proteins such as protein A, protein G or protein L by functionalizing CNTs with

appropriate antibodies [37, 38]. The results from such research work may turn out to be fruitful in elucidating several other biological mechanisms like antibody-antigen attachment, immobilization of protein and DNA melting [39, 40].

The rationale of pursuing an integrated approach combining microfluidic lab-on-a-chip devices with shear enhanced flow is to establish the path towards development of mAb antibody purification without post-modification damages. This device should outperform traditional systems both in their portability, yield, and capture efficiency [41]. The packing of the CNT inside the microchannel should have unprecedented high surface to volume areas, large and sensitive electrical signal, and customizable surface chemistries, and therefore serve as an ideal platform to build novel mAb analysis systems [42]. Also, the frequency and waveform tunability of the EIS signals from the interdigitated electrodes will make them especially suitable for engineering novel approaches to carry out simultaneous affinity and efficacy testing of the antibodies. This lab-on-a-chip device is an integrated approach for studying, analyzing and purifying monoclonal antibodies in situ [43].

In this report, Chapter 2 introduces mAbs, its use in therapeutic and biomarker studies. Chapter 2 discusses in details the desired degree of purification needed for mAb, along with the advantages and disadvantages of current methods to purify mAbs. The mechanism and the chemistry involved during purification of mAbs are also highlighted.

Chapter 3 introduces the basic EIS principles, EIS data interpretation, classical EIS circuit models and the concept of RC time or relaxation time, which is a unique property of an interface. [12]. In an electrochemical system, two simultaneous phenomena can take place at the electrode-electrolyte interface. These are charge storage (kinetic controlled) at

the interface or charge transfer (mass transfer control) across the interface. The RC time at the interface in conjunction with the frequency of the applied field determines the dominating physical phenomenon. The discussion on RC time is followed by a brief discussion on the implementation of EIS in microfluidic devices in existing literature. Chapter 4 sheds some light on both the experimental protocols that were followed during the entire study and the data. First, the Nyquist plots obtained for both continuous and batch process are described in this chapter to show the enhanced sensitivity and the departure from classical results for the continuous process. The protocols involve CNT oxidation, chip fabrication, on-chip surface activation of CNT surface and mAb-pAb attachment to CNT complex. The results are analyzed in details, and their departure from classical equivalent circuits are examined. Finally, a model to fit the EIS data to an equivalent circuit is discussed.

CHAPTER 2

PURIFICATION OF MONOCLONAL ANTIBODY

In this chapter, mAbs are introduced with a discussion about its use in therapeutic and biomarker studies. Further, the different methods for antibody purification along with their advantages and disadvantages are discussed here. The desired degree of purification is also discussed. Further, the mechanism and the chemistry involved in the purification of the monoclonal antibody is discussed in details.

2.1 Monoclonal Antibody: An Overview

Monoclonal antibodies are the fastest growing area of research and study in the field of therapeutic drug and biomarkers in pharmaceuticals. The effectiveness of mAb usage in sensing platform stems from their high specificity and high affinity towards the targets. mAbs are large (~150-450 kDa) Y-shaped molecules with a complex three-dimensional structure composed of four polypeptide chains [45]. The structure also comprises of two heavy chains (~50 kDa each) and two light chains (~25 kDa each) [44]. Both heavy chains and the light chains consist of variable and constant domains. The mAbs have two basic functional units, the ‘Fragment antigen-binding (FAB) region and the fragment crystallizable (FC) region[45]. The Fab fragments have two amino-terminal ends while the FC fragment is referred to as the stem or carboxyl-terminal end [45].

There are many subclasses of mAbs like, IgA, IgD, IgE, IgG, IgM where the name is synonymous with the amino acid sequences of the heavy chain [46]. However, most

therapeutic mAbs belong to the IgG subclass. A typical mAb molecule (the prototype class of immunoglobulin is IgG) is made up of two identical antigen-binding sites at the ends of its Y arms[47]. The light and heavy chains contribute to the binding of antigens. Each antibody molecule is capable of binding with two identical antigens. The stem of the Y is known as the "hinge region" where the two arms meet [48]. The hinge region introduces segmental flexibility of the antibody molecule [48]. The amino-terminal end of an antibody is called the variable or V region, while the carboxyl-terminal end is called the constant or C region [49]. The C region is about the same size as the V region in the light chain, while the C region is about three to four times larger than the V region in the heavy chain. The V

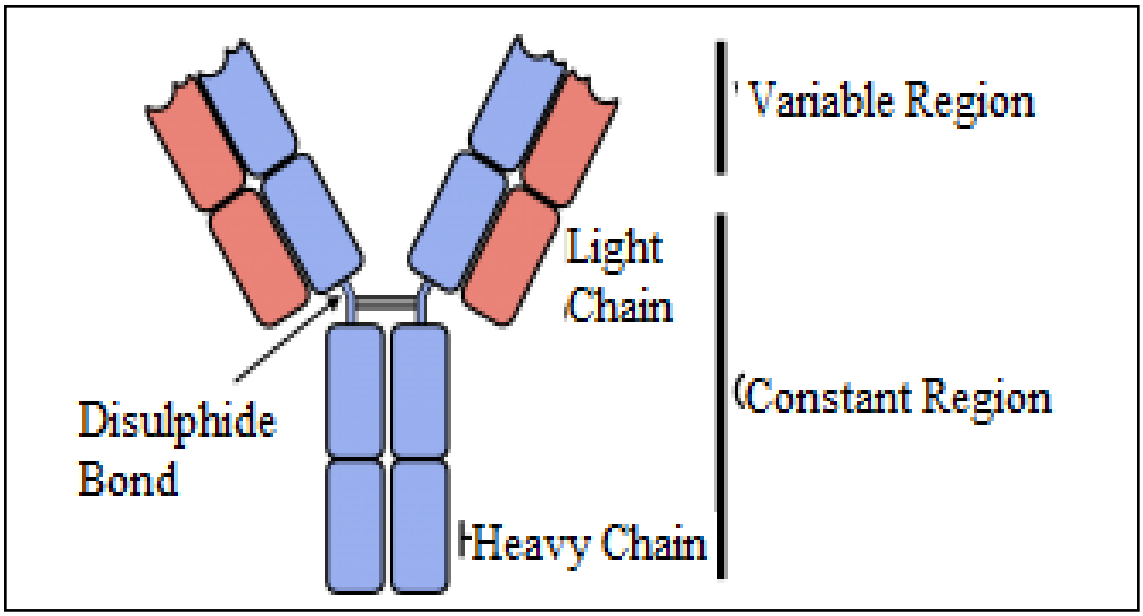

Figure 2.1 A typical schematic of a monoclonal antibody consisting of a pair of "heavy chains" that creates and maintains the antibodies overall protein structure, and two "light chains", which recognize and bind specific antigens. The genes for light chains are hypervariable**.** The CDRs come together at the amino-terminal end of the antibody molecule to form the antigen-binding site, which determines specificity.

regions of light and heavy chains are responsible for forming the antigen-binding sites[48]. Structurally, light and heavy chains consist of repeating, similarly folded domains. The light chain has one V-region domain and one C-region domain, whereas the heavy chain has one V region and three or four C region domains. Most of the variable parts of the V regions are limited to several small hypervariable which are complementarity-determining regions (CDRs)[50]. The three CDRs in the light and heavy chains come together at the

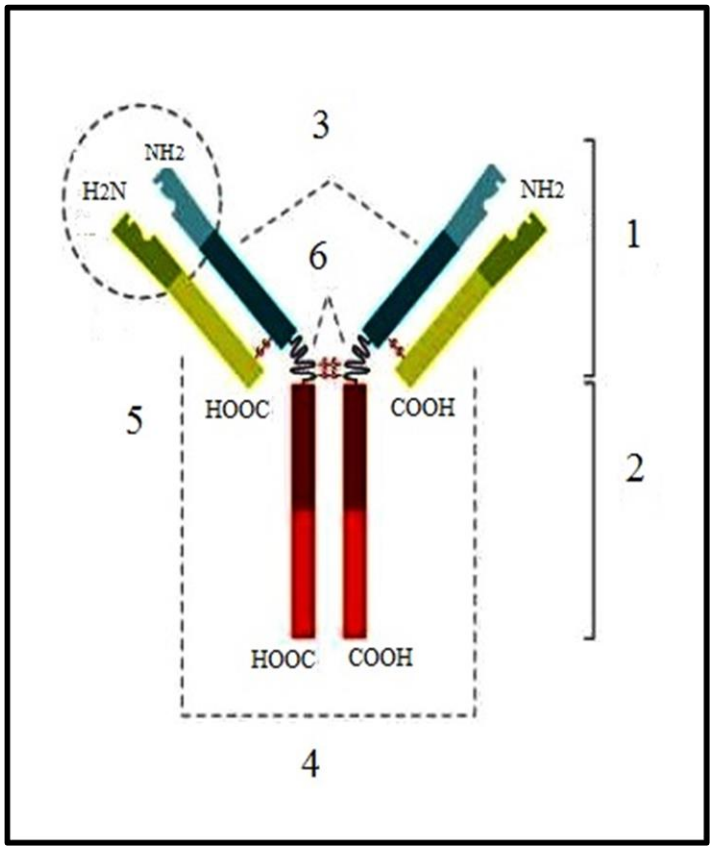

Figure 2.2 A schematic diagram of a monoclonal antibody demonstrating 1) FAB region 2) FC region 3) Heavy chain with one variable domain V followed by a constant domain C and a hinge region and to more constant domains. 4) Light chain with one variable and one constant domain region 5) Antigen binding site 6) Hinge regions.

amino-terminal end of the antibody molecule to form the antigen-binding site, which determines specificity [50].

2.2 Monoclonal Antibody in Cancer Therapeutic and Biomarker Research

Antibodies are a vital part of the immune system. Normally, antibodies get activated in response to a foreign material i.e. antigen (such as a protein in a germ) entering the body [25]. The antigen attaches to the antibody to neutralize the effect of antigen and prevent the antigen from causing undesirable changes in the human body [51]. Over the years, scientists having to work on analyzing specific antigens, like those on the surface of cancer cells (target) to introduce an antibody that matches the specific antigen. Here, the ability of mAbs to be extremely specific to their target molecule is used for the treatment of cancer[52]. Thus the monoclonal antibodies are a relatively new type of "targeted" cancer therapy. This uniqueness in specificity also allows mAbs to be used as a potential biomarker for sensors and diagnostic devices [53]. Hence, the chemical structure of antibodies explains the three critical functions of antibodies [52, 54, 55]:

(1) Binding versatility

(2) Binding specificity

(3) Biological activity

Studies reveal that some animal and plant species are capable of responding to more than 100 million antigenic determinants and can even respond to artificial antigens that are non-existent [56]. Owing to the amino acid sequence variation in the arms of antibody molecules, each different antibody can bind specifically to one unique antigen [51]. All these features have allowed mAbs to be the driver behind the immunologic research and answering many basic and clinical questions associated with immunotherapy [57].

Cancerous cells, unlike normal human cells, go through rapid cell division causing various side effects. Till date, research on cancer treatment has primarily focused on the killing of this rapidly dividing cancer cells. Some of the methods for destroying cancer cells are near-infrared photothermal therapy (NIR), radio frequency ablation, plasma-and ultrasound-induced destruction [58-61]. Thus there has been a sustained research push over the last few decades in cancer treatment towards ‘Targeted therapy.' Targeted therapy is about identifying cancer cells by understanding the physic-chemical, cellular level dynamics, proteins on the surface and molecular pathway differences between cancer cells and normal human cells [62].

The major challenge revolves around attacking the cancer cells without damaging the normal cells. Invasive methods such as radio-frequency ablation, besides killing the cancerous cells also injures or **kills normal cells** and tissues. However, mAbs can initiate an immune system response that can destroy the outer wall (membrane) of a cancer cell [54]. They block the connection between a cancer cell and cell growth promoting proteins. For the growth and survival of a cancerous tumor, continuous blood supply is needed. Some mAb drugs block protein-cell interactions often necessary for the development of n new blood vessels [63]. Certain proteins called regulators can bind to the immune system and prevent hyperactivity of the system. Further, the attachment of mAbs to a cell can lead to the self-destruction of a cancerous cell [56].

Mabs can be designed as a delivery vehicle. For example, in a variation of radioimmunotherapy, attaching a small radioactive particle to a mAb transports the radiation treatment directly to target cells. This minimizes the effect of radiation on healthy

cells [64, 65]. Similarly, mAbs attached to a chemotherapeutic drug can deliver the treatment directly to the cancer cells while maintaining avoidance to healthy cells

2.3 Methods of Purification

In this section, various techniques currently used for the purification of mAbs are discussed along with their advantages and disadvantages.

2.3.1 Salt Precipitation (Ammonium Sulfate)

Ammonium sulfate precipitation is one of most widely used methods for removing proteins in solution [66]. Proteins in aqueous solutions form hydrogen bonds with water due to the polar and ionic groups on the solution. Highly charged small ions such as ammonium and sulfate when added in large concentrations compete with proteins for binding with water [66]. This prevents the hydrogen bonding between the protein from the water molecule, resulting in a decrease in its solubility and precipitation. However, this method has a much poorer yield compared with all the other available methods. Factors affecting protein precipitation are the number of polar groups, the precipitation temperature, the solution pH and the molecular weight of the protein. The concentration of ammonium sulfate at which antibodies precipitate varies with antibody type [66]. Further, post sulfate precipitation, the resulting antibodies are also contaminated by high molecular weight proteins. Hence, this purification method is unsuitable when high yields, high purity is required or no post-modifications are required.

2.3.2 DEAE Ion exchange (Batch Chromatography)

Ion exchange chromatography has a very widespread use for antibody purification and is often applied as the second step post ammonium salt precipitation [67]. The principle of ion exchange chromatography works by utilizing the differences in the isoelectric points of antibodies and other serum proteins [67]. The antibodies bind to the column when the pH of the column (like anion exchange column such as DEAE cellulose) is reached below the isoelectric point of antibodies. Though the antibody purity from DEAE chromatography is slightly better than ammonium sulfate precipitation, it is still low when high purity is a requirement [67]. Depending on the level of antibody purity required, DEAE chromatography has to be coupled with further purification steps. Hence, DEAE chromatography is almost always costly as it is a multiple step purification method [67].

2.3.3 Caprylic Acid

Short-chain Caprylic acid under mildly acidic conditions precipitates most of the serum proteins except for IgG molecules [68]. This type of precipitation is useful when large volumes are used [68]. However, this purification process yields impure antibody fractions [68]. Hence, to enhance collection efficiency, the caprylic acid method has to be coupled with other purification steps, such DEAE ion exchange chromatography [66].

2.3.4 Hydroxyapatite Chromatography

A comparatively rapid and efficient process for large scale purification of antibodies is column chromatography on hydroxylapatite [70]. In this method, antibody yields are high, and the level of purification achieved is also good. Serum from hyperimmune animals or

with ascites fluid (from mAb production) is used here. Even if the purification degree with hydroxylapatite chromatography is quite high, this preparative step has to be coupled with other purification steps [70]. Further, this method always results in high post-modifications in atibodies [70].

2.3.5 Gel Filtration (Sephadex, Sepharose)

Gel filtration on Sephadex or Sepharose (medium-sized beads, exclusion limit of 300,000 to 500,000 daltons for globular proteins) is useful for the separation of antibodies of the IgM isotype [71]. These molecules are relatively larger than IgG antibodies and other molecules in serum and facilitate separation [71]. Nevertheless, gel filtration has to be combined with other methods, such as, ammonium sulfate precipitation to obtain highly pure antibodies [71].

2.3.6 Antigen Affinity

Immuno-affinity chromatography on an antigen column is the most popular and most effective method to purify antigen-specific antibodies from serum, ascites fluid or culture media [70]. In this procedure, water-insoluble immune-adsorbents are prepared by covalent coupling of pure antigen to a solid supports [28]. One of the most popular methods is coupling antigen to cyanogen bromide activated agarose beads. These beads are subsequently filled into a column. The antibodies specific to the antigen are allowed to bind; unbound antibodies and contaminating proteins are removed by several washes. Finally, specific antibodies are eluted by low and high pH buffer cycles [28]. High-affinity antibodies may not elute under these conditions. Elution with chaotropic ions (e.g. KSCN)

is done then [28]. The major advantage of immunoaffinity chromatography is the unique ability to isolate antibodies from a mixed pool [28]. The disadvantages of this method are the requirement of large quantities of pure antigen and secondly, the elution conditions can lead to the loss of antibody by inactivation [28].

2.3.7 Capillary Isoelectric Focusing

One method that has merged the advantages of microfluidics with chromatographic separation techniques for highly reproducible results of monoclonal antibody purification and specificity analysis is Capillary isoelectric focusing (CIEF) [71]. CIEF characterizes the charge of the proteins and separates the different charges according to their isoelectric points (pI), the characteristic pH at which the net electric charge is zero [72]. Though multiple methods for CIEF exist in literature, most methods consist of filling the microfluidic channel or a capillary with a mixture of protein sample and ampholytes followed by application of a high electric field [24, 71-73]. The ampholytes constitute a pH gradient in the capillary, and the proteins are focused into the pH region that corresponds to their P_I [72]. The contents of the capillary are then mobilized past the detector by applying pressure to the inlet vial while maintaining the field strength. However, CIEF, using electrophoretic methods often adversely affect the structure and thus the function of the mAbs [74]. One major issue of this technique is that it is sensitive to high salt concentration and would result in a bad separation of protein charge variants [75]. Further, CIEF is highly susceptible to high protein levels in the sample. The final protein concentration which can be injected into the sample-ampholyte mixture, depends on the solubility of protein components and the sensitivity requirements [75]. The high

hydrophobicity and high molecular weight of antibodies often lead to precipitation during focusing at low concentrations [74]. High ionic strength can also negatively influence the process, causing long focusing times and mobility peak broadening [76].

The most advanced techniques of chromatography column separation such as Protein A affinity chromatography has been shown to be highly selective for mAbs, resulting in >95% purity [71]. The method entails the addition of a mixture of proteins to the column where the antibody specifically binds its target protein and retains itself on the column while other proteins are washed away [77]. The target protein can then be removed from the resin by a salt solution or buffer. However, the use of an immobilized protein as a ligand creates separation challenges; the ligand is prone to proteolysis, and this breakdown can cause its pieces to adhere to product molecules, thus creating a separation challenge. Additionally, the Protein A ligands cannot be exposed to alkaline conditions that are used to purify other column designs and require the use of high concentrations of chaotropic, creating a cost and disposal challenge [28]. Implementing this technique with low ligand removal requires considerable effort in development and is hard to implement into the routine analysis and regulated quality control. Implementing chromatographic methods in the later stages, when the sample size is smaller can make it feasible, but cannot guarantee high purification [67, 69, 78]. Additionally, the antigen molecules may suffer from many physical and chemical stresses during the process, introduce aggregation of mAbs and oxidation of tryptophan - creating shorter retention time of the antibody with oxidized tryptophan on the column, suggesting less hydrophobic interactions of the molecules with the chromatography process.

In the table below the existing methods for the purification of monoclonal antibody along with their advantages and disadvantages are summarized [28, 71, 85]:

Table 2.1 Methods of Purification of MAbs along with their Advantages and Disadvantages

Method	**Application, quality**	**Advantage**	**Disadvantage**
Ammonium Sulfate	Bulk of serum γ-globulins Useful for concentration, not recommended as single step	Easy, cheap convenient for large volumes Low loss of antibodies	Poor purification degree must couple with another purification step
DEAE Ion Exchange	Partial purification, not recommended as single step	Cheap and convenient for large volumes and concentration	Impure antibody fractions (but higher than with ammonium salt), must couple with another purification step
Caprylic Acid	Moderately pure IgG, not recommended as single step	Cheap and convenient for large volumes	Impure antibody fractions must couple with another purification step

Hydroxylapatite	Relatively pure antibodies, not recommended as single step	High yield of concentrated antibodies	Impure antibody fractions must couple with another purification step
Gel filtration	Separation by molecular mass, not recommended as single step	Relatively pure separation of IgM from other antibody molecules	Low capacity High dilution of antibody fraction, not useful for IgG antibodies
Protein An affinity	Pure IgG with species and isotype selectivity Single step method	High purification degree High yield	Not suitable for all species and isotypes
Antigen affinity	Pure antibodies by selective antigen method Single step method	High specificity and purification degree High yield	Pure antigen required Method associated with loss and inactivation of antibodies by elution procedure

2.4 Post Modifications in Antibody

Existing purification methods like affinity chromatography, GC, HPLC can lead to undesirable post modifications of antibodies. Post-transitional modifications are structural and chemical changes including cleavage of the peptide as a result of their covalent

attachment to functional groups or proteins during purification [79]. As these modifications alter the structure of antibodies, it affects their activity, stability, localization and interacting partner molecules[80]. Chemical alterations that usually occur during the post-translational modification of antibodies include phosphorylation, methylation, acetylation, ubiquitination, nitrosylation, glycosylation, and lipidation [81]. Antibody Glycosylation is a common post-translational modification and has a critical role in antibody effector function. The modified molecule demonstrates unusual behavior during development due to the alteration of its intrinsic properties and stability. In therapeutic cancer treatment post modification is undesired as it alters the structure of the antibody [82].

2.5 Antibody Attachment Mechanism

The primary reason for choosing **Carbon nanotubes** (CNTs) as the binding platform for antibodies is owing to several thermal and mechanical properties [43]. These allow CNT's to be used in a wide variety of applications in nanotechnology, electronics, optics and other fields of materials science [20]. Recent studies indicate that the CNTs brought down to sizes in the range of 1-100nm exhibit unique electrical, optical, chemical and pharmaceutical properties like high electrical conductivity, high tensile strength and flexibility and low thermal expansion coefficient [42]. Carbon nanotubes (CNTs) have a significant impact on the development of newer methodologies and devices useful for the analysis and the detection of various types of biomolecules such as DNA, protein, antigens, antibodies [43]. The detection sensitivity can be increased many folds in comparison to existing methods such as GC, HPLC. The extraordinary properties of carbon nanotubes have led to the demonstration of several applications of CNTs. However, commercial

realization of these CNTs and CNTs based devices require consistent quality of CNTs and these should be free of any impurity. The major advantages of nanostructured materials are listed below [42]:

- Better sensitivity
- Amplified electrical signal
- Help improve the mobility of macromolecules to the surface of the antibody-functionalized electrodes
- Provide a unique confined environment for a particular macromolecule-specific-captured antibody to interact with pharmaceutical molecules.

Controlling the covalent binding of antibodies onto functionalized carbon nanotubes is a key step in the design and preparation of nanotube-based microfluidic devices A mAb is linked to either multi-walled (MWCNTs) or double-walled carbon nanotubes (DWCNTs) using different attachment chemistries[83]. Two types of strategies have been reported To run conjugation of the immunoglobulins (Ig) to CNTs, [83]:

1) Covalent bonding

2) Non-covalent interactions

A covalent bond offers good stability and better binding selectivity due to its ability to directly control the location of the antibody [23]. On the contrary, a noncovalent interaction between an Antibody and the nanotubes may lead to conjugates with insufficient stability and selectivity [46]. Further in noncovalent interaction, the antibody is linked to a polymer adsorbed onto the CNT surface [84]. This approach limits the use of

the conjugates *in-vivo* because the polymer can be displaced by other biological macromolecules resulting in dissociation of the Ig protein from the nanostructure [85].

One of the key steps during introducing the covalent bond is surface activation. NHS and Sulfo-NHS are commonly used to prepare amine-reactive esters of carboxylate groups for chemical labeling, crosslinking and solid-phase immobilization applications [86]. Carboxylates (-COOH) reacts with NHS or Sulfo-NHS in the presence of a carbodiimide such as EDC forming a semi-stable NHS or Sulfo-NHS ester [87]. This reacts with primary amines (-NH2 present in antibodies) to form amide crosslinks. The usage of NHS or Sulfo-NHS enhanced the coupling efficiency of carbamide reactions. Both NHS and Sulfo-NHS are soluble in aqueous and organic solvents [87]. However, NHS activation decreases water-solubility of the modified carboxylate molecule. The charged sulphonate group in sulpho-NHS increases activation as it preserves or increases water-solubility of the modified molecule [87]. Although prepared NHS or Sulfo-NHS esters are sufficiently stable to process in a two-step reaction scheme, both groups will hydrolyze within hours or minutes, depending on water content and pH of the reaction solution. NHS esters have a half-life of 4-5 hours at pH 7, 1 hour at pH 8 and only 10 minutes at pH 8.6. Hence, the best results are obtained when NHS-activated molecules are used promptly for reaction to the amine-containing targets [88]. The activation reaction with EDC and Sulfo-NHS is most efficient at pH 4.5-7.2. EDC reactions are performed in PBS buffer at pH 7.5. The response of Sulfo-NHS-activated molecules with primary amines is most efficient at pH 7.2-8. Sulfo-NHS-ester reactions are usually performed in phosphate-buffered saline (PBS) at pH 7.2-7.5 [88]. The attachment of mAbs with Protein A is one of the major **steps in** monoclonal antibody purification [88]. It is important to understand the mechanism of

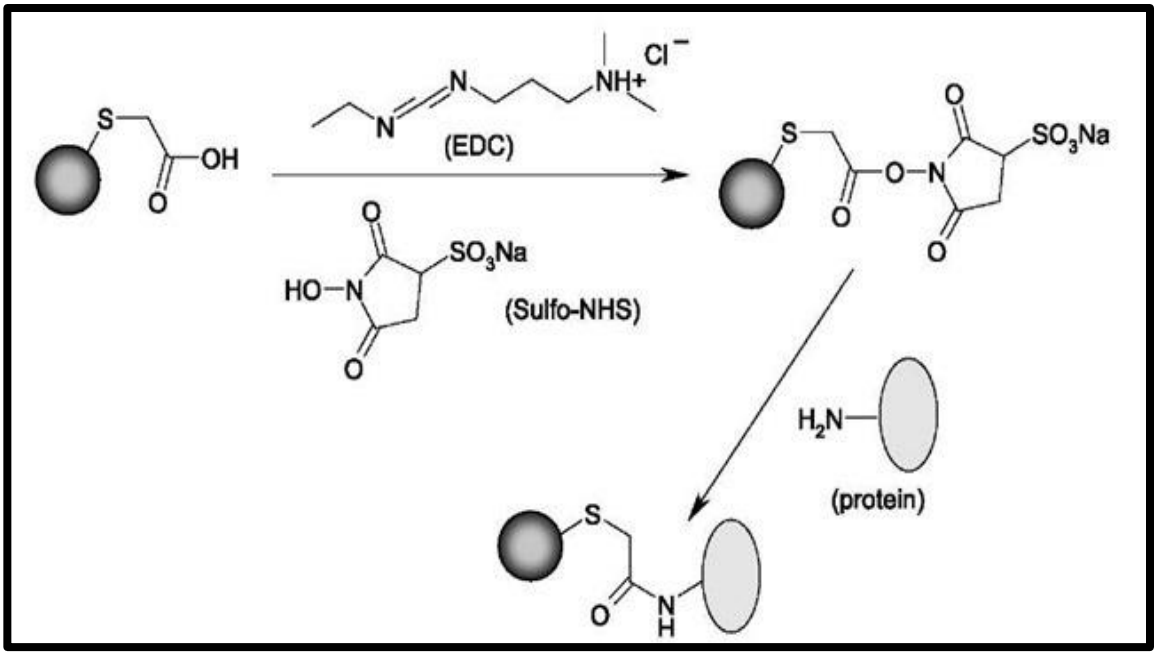

Figure 2.3 Schematic of the Sulfo-NHS/EDC conjugation reaction. Carboxylates COOH) reacts with NHS or Sulfo-NHS in the presence of a carbodiimide such as EDC forming a semi-stable NHS or Sulfo-NHS ester. This reacts with primary amines (-NH2 present in antibodies) to form amide crosslinks.

mAbs-Protein attachment. Protein A binds to the FC region of IgG molecule around the hinge, which contains five highly homologous FC-binding domains and binds at least two IgG molecules simultaneously. The precise region of the FC that binds to protein A can also bind to other molecules such as protein L or protein G [89]. Hence, it is called consensus binding site (CBS). The CBS is largely hydrophobic in character, with relatively few polar residues and has a high level of solvent accessibility[89]. These features indicate burial of hydrophobic residues as a strong driver of binding and electrostatic interactions [89]. Hydrogen bonds at certain highly conserved sites have also been indicated in binding. According to Delano et al., the CBS undergoes considerable conformational changes when binding to a ligand [90]. In fact, the nature of the change in

conformation depends on the ligand, highlighting the flexibility of this region. Even though flexibility implies good structural recovery after the conformational change, under antagonistic conditions such as low pH there may be greater vulnerability to detrimental levels of structural alteration [90].

CHAPTER 3

PRINCIPLES OF ELECTRONICIMPEDANCE SPECTROSCOPY

This chapter deals with the basic principles of EIS are elaborated in details. Details on EIS data interpretation and the concept of RC time constant is introduced. The basic EIS circuit models are also introduced. Finally, the usage of EIS in microfluidic devices is discussed in detail.

3.1 Background

The concept of electrical impedance was first introduced by Oliver Heaviside in the 1880s [15]. In EIS, unlike general electrical circuits, the circuit elements represent complex physics behavior. Electrical impedance is the response from a system on application of an alternating current (AC) voltage signal V (Volt) with small amplitude V_A applied at a frequency f (Hz). Hence unlike in direct current (DC) where the primary resistance to current is resistance, in AC the same resistance to current flow is called Impedance [12]. The AC voltage signal V(t) expressed as a function of time t is given by equation (1) [12]:

$$V(t) = VA\sin(2\pi ft) = VAsin(\omega t) \quad \text{……...……..….(3.1)}$$

where ω the radial frequency of the applied voltage is $2\pi f$ where f is the frequency of the applied AC signal. The current response I(t) to a sinusoidal voltage input remains a sinusoid at the same frequency, however, with a phase shift Φ. If I_A is the current amplitude, then $I(t)$ can be expressed as in equation (2),

$$I(t) = IA\ sin\ (\omega t + \Phi) \quad \text{…….. (3.2)}$$

The complex impedance is calculated by taking the ratio of input voltage V(t) and the output current I(t) as follows akin to Ohms' Law for DC circuits.

$$Z = V(t) / I(t)$$

$$= V_A \sin(\omega t) / I_A \sin(\omega t + \Phi) \quad \text{(3.3)}$$

$$= Z_A \sin(\omega t) / \sin(\omega t + \Phi)$$

where Z_A is the absolute value, $Z_A = |Z|$. The impedance can also be represented in Euler notation as having a 'real' or in phase (Z_{Real}) and 'imaginary' or 'out of phase' (Z_{Im}) component as in equation 4.

$$Z = Z_{Real} + jZ_{Im} \quad \text{(3.4)}$$

Where the phase angle Φ is related to the impedance as $\tan \Phi = \frac{Z_{Im}}{Z_{Real}}$

For a resistor (R) and a capacitor (C) circuit in series the equivalent Impedance is,

$$Z_1 = R$$

$$Z_2 = \frac{j}{\omega C}$$

$$Z = Z_1 + Z_2 = R + \frac{j}{\omega C} \quad \text{(3.5)}$$

If the same resistor (R) and a capacitor (C) as above is in parallel then the equivalent circuit is,

$$Z = \frac{R}{1 + (\omega RC)^2} - j\frac{\omega R^2 C}{1 + (\omega RC)^2} \quad \text{(3.6)}$$

Here, C = capacitance, R= resistance

3.2 EIS Data Interpretation

To interpret EIS into relevant physical processes, it is critical to describe an equivalent circuit that has an equivalent impedance similar to that observed from experiments. An equivalent circuit can be composed of a multitude of resistances and capacitances, like a parallel combination of capacitance and resistance or a series combination of capacitance and resistances [90]. To describe the process of fitting an equivalent circuit to an impedance model here is described the simplest form of an equivalent circuit, the Randles circuit. The Randles circuit defines the simplest system possible which is two electrodes dipped in an electrolyte. It consists of an active solution resistance R_S in series with the parallel combination of the double-layer capacitance C_{dl} and a faradaic resistance R_{CT} [90]. Often a Constant phase element (CPE) is used in place of the double layer capacity (C_{dl}) [91]. In the two electrode system, there are two separate regions, namely, the bulk and the interface. The solution resistance Rs is a representation of the conductivity of the electrolyte and any resistance in the wires used to measure EIS. At the electrode interface, there are multiple paths for the ions in the solution. The ions can either collect near the interface as a charge storage mechanism, or they can react (Faradic Reaction) with the electrolytes. The storing of charge at the electrode-solution interface is called the Electrical Double Layer or the Debye Layer and is designated as C_{dl} in the equivalent circuit [36]. This double layer is formed as ions from the solution adsorb onto the electrode surface [12]. The magnitude of the double layer capacitance depends on many variables such as electrode potential, temperature, ionic concentrations, types of ions, oxide layers, electrode roughness and impurity adsorption [3, 12, 36]. The faradic resistor is represented as the charge-transfer resistance R_{CT}. The Faradic resistor often leads to a depletion of ions at the interface. This results in the formation of a diffusive gradient from the bulk to the interface. This is

represented as the Warburg Element, W_D, in the circuit. At higher frequencies, the Warburg impedance tends to be smaller since reactants are not allowed to have enough time to diffuse[79]. While at lower frequencies, the reactants get adequate time to diffuse leading to an increase in the Warburg impedance. For a linear system, the Warburg impedance appears as a straight line with a slope of 45° in a Nyquist Plot [80]. While on a Bode Plot, the Warburg impedance exhibits a phase shift of 45° [80].

There is an electrical double layer that exists on the interface of an electrode and its surrounding solution [79]. This double layer forms as ions from the electrolyte solution accumulate on the electrode surface. Along with the solution resistance, R_s and charge resistance R_{CT}, diffusion also occurs accompanied by another impedance called a Warburg

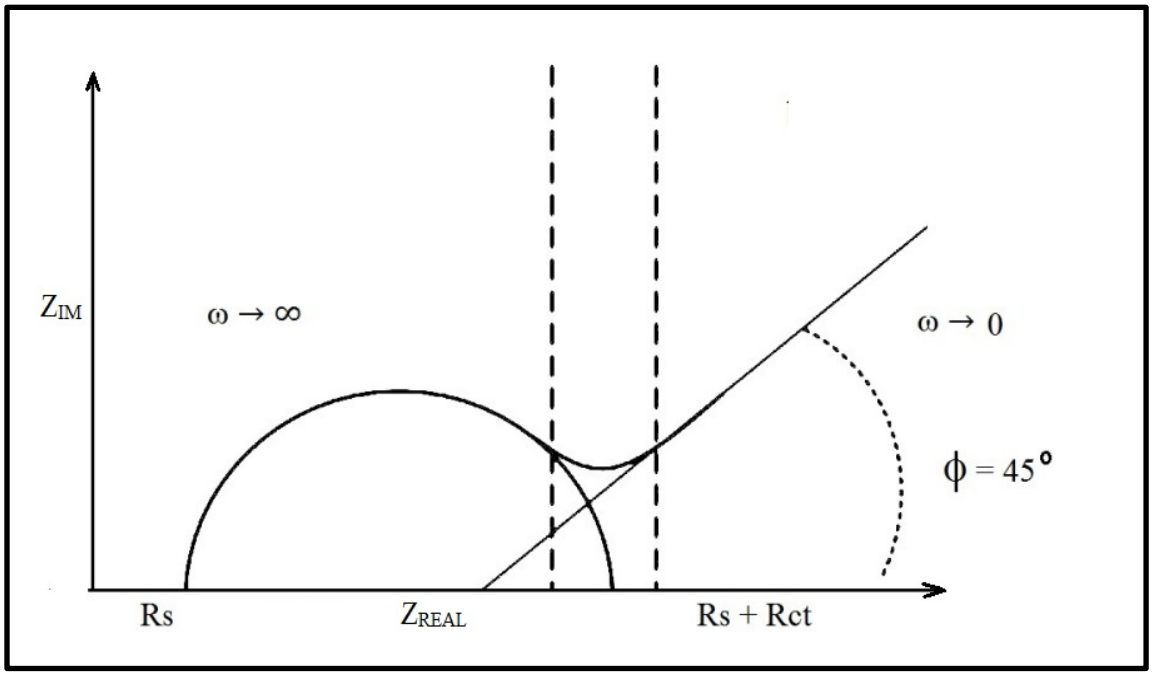

Figure 3.1 A typical Nyquist Plot showing a) the capacitive nature of a system at higher frequency b) the resistive nature of a system at lower frequency followed by an equivalent circuit diagram of the system. the impedance is represented as a vector of length $|Z|$. The angle between this vector and the x-axis is the phase angle Φ and the Warburg impedance appears as a straight line with a slope of 45°.

impedance R_W. This impedance primarily depends on the frequency of the AC potential applied [79].

The fitting of the model to the experimental data should be performed using complex nonlinear least-squares procedures available in various EIS data fitting computer programs to obtain the Randles circuit parameters [13]. The Randles equivalent circuit is one of the simplest possible models describing processes at the electrochemical interface. In real electrochemical systems, impedance spectra are usually more complicated and, thus, the Randles circuit may not give appropriate results [13].

A Nyquist plot is a complex plane impedance diagram, where (Z_{IM}) is plotted against (Z_{Real}) [12]. In the Nyquist plot, the high-frequency region is closer to the origin while the lower frequency area is further from the origin. At high frequencies, the impedance of the system is chiefly capacitive, while at the lower frequency the impedance is chiefly resistive in nature. The Nyquist plot for a Randles cell is always a semicircle [13]. The solution resistance can found by reading the real axis value at the high-frequency intercept. This is the intercept near the origin of the plot. The real axis value at the other (low frequency) intercept is the sum of the polarization resistance and the solution resistance. The diameter of the semicircle is, therefore, equal to the polarization resistance. Alternatively, the EIS data can be interpreted using a Bode diagram. Bode plots are a very useful way to represent the gain and phase of a system as a function of frequency. This is referred to as the frequency domain behavior of a system. One of the most commonly used test functions for a circuit or system is the sine wave [36]. The impedance is plotted with log frequency on the x-axis and both the impedance and phase shift on y-axis [36].

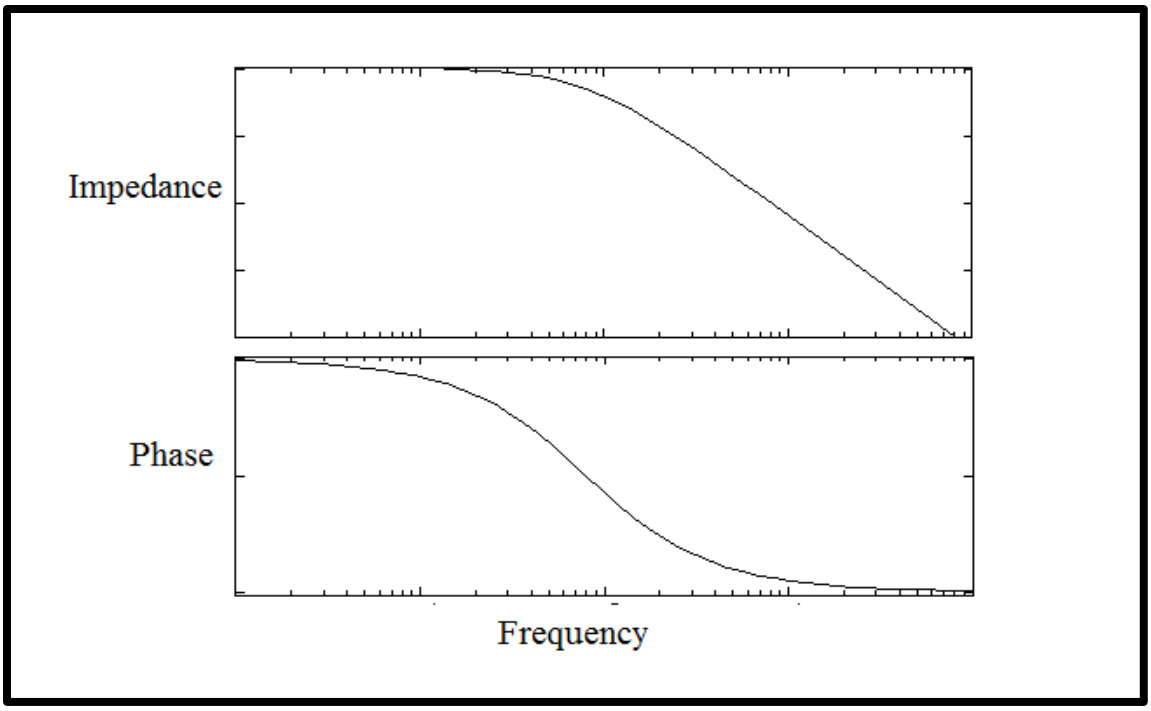

Figure 3.2 Bode plot, showing the frequency domain behavior of a system. The impedance is plotted with log frequency on the x-axis and both the impedance and phase shift on y-axis

A capacitor's impedance decreases as the frequency increases [36]. Capacitors also have an imaginary impedance component. The capacitive current follows a 90 ° phase shift on the voltage. The electrochemical systems modeled as a network of passive electrical circuit elements is called an "equivalent circuit." The EIS response of an equivalent circuit can be calculated and compared to the actual EIS response of any electrochemical system. Two common classical electrochemical equivalent circuits that will be encountered during the experiments described in the next chapter are described here.

Mixed Kinetics Controlled Diffusional Model

The mixed Mixed Kinetics Controlled Diffusional Model takes both diffusion and mass transfer into account. This model is same as the Randles circuit but always with a Warburg

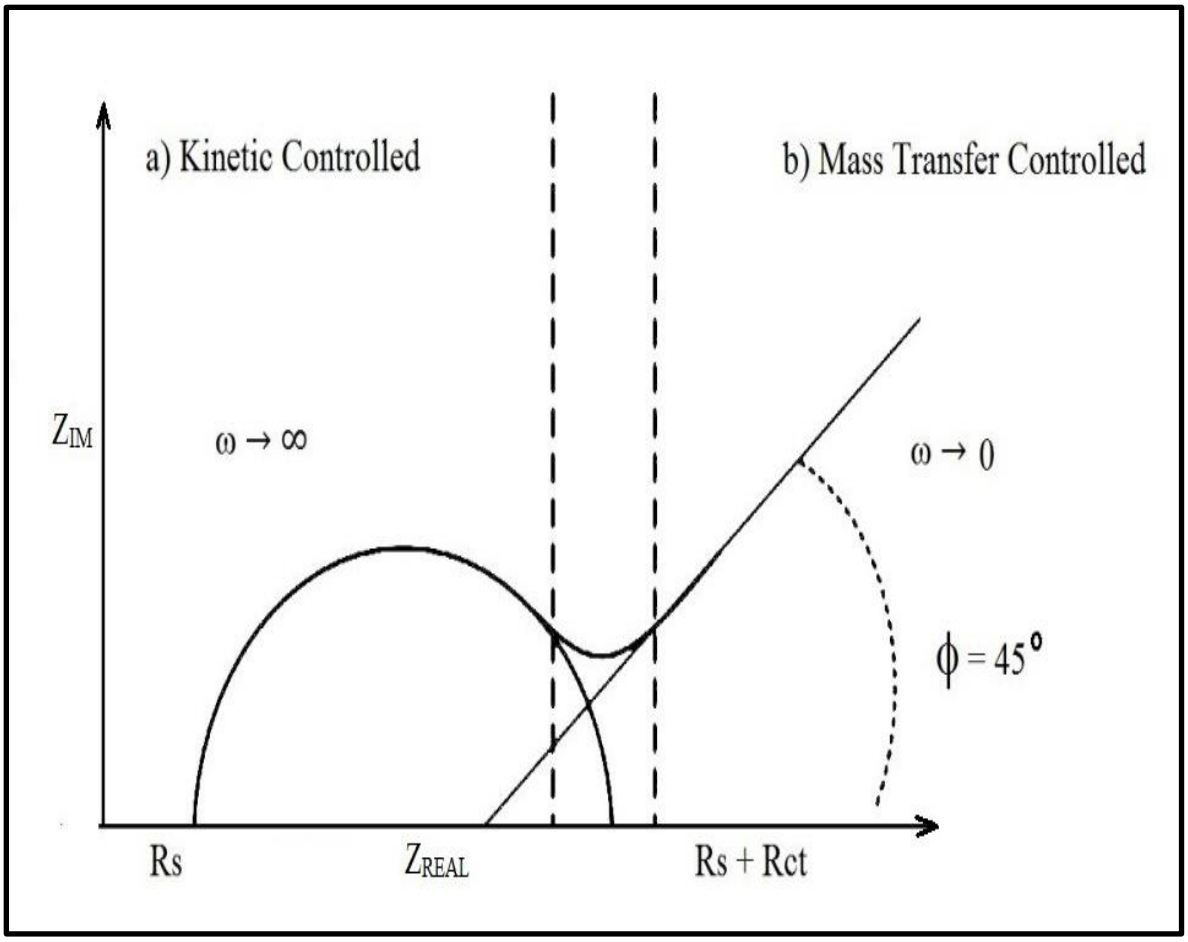

Figure 3.3 Nyquist plot for a mixed kinetic control circuit where the impedance is represented as a vector of length $|Z|$. The angle between this vector and the x-axis is the phase angle Φ and the Warburg impedance appears as a straight line with a slope of 45°.

impedance [13]. An example of a simple kinetic controlled situation is PBS flowing through a 100 nm wide channel in a microfluidic device with Ti-Au microelectrodes, the Warburg element manifests itself in EIS spectra by a line with an angle of 45 degrees in the low-frequency region. Values of the charge transfer resistance and Warburg coefficient depend on physicochemical parameters of a system under investigation [91].

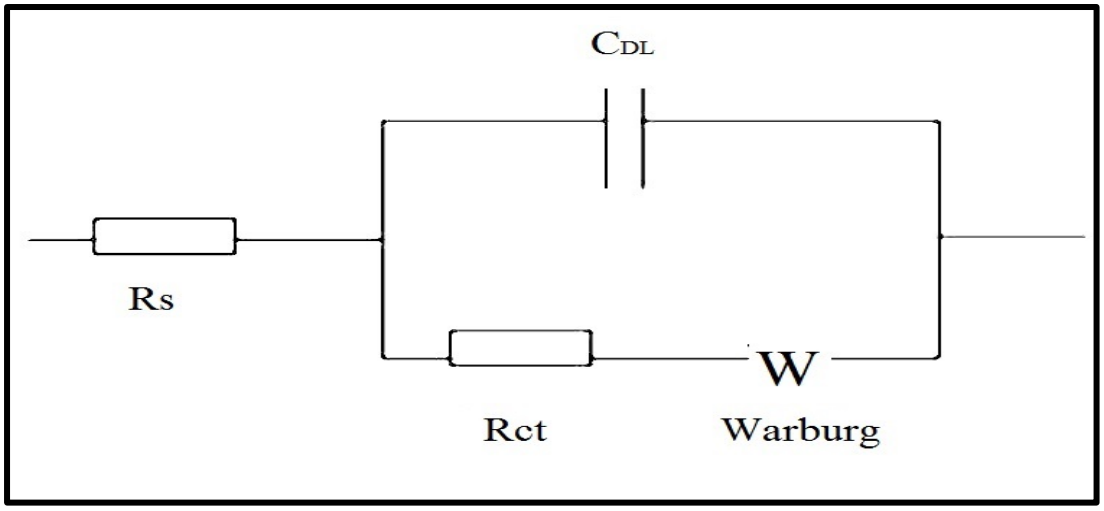

Figure 3.4 The equivalent circuit for mixed kinetics and diffusion model. The model consists of the impedance of a faradaic reaction that consists of an active charge transfer resistance R_{ct} and a specific electrochemical element of diffusion W, which is also called a Warburg. The capacitor is denoted by C_{DL} which is parallel to the resistors

Voigt Model

Voight model is usually encountered whenever there are coatings on the electrodes, and the system works as a multi-electrode system [13]. If we seek into the morphology of a bacterial cell in the electrolyte, there are tortuous paths in between. These paths may be physical pores filled with electrolyte. On the metal side of the pore, an area can be assumed of the bacteria that delaminates and a pocket filled with an electrolyte solution forms [13, 91]. This electrolyte solution can be very different from the bulk solution outside of the bacterial cell. The interface between this pocket of the solution and the bacteria is modeled

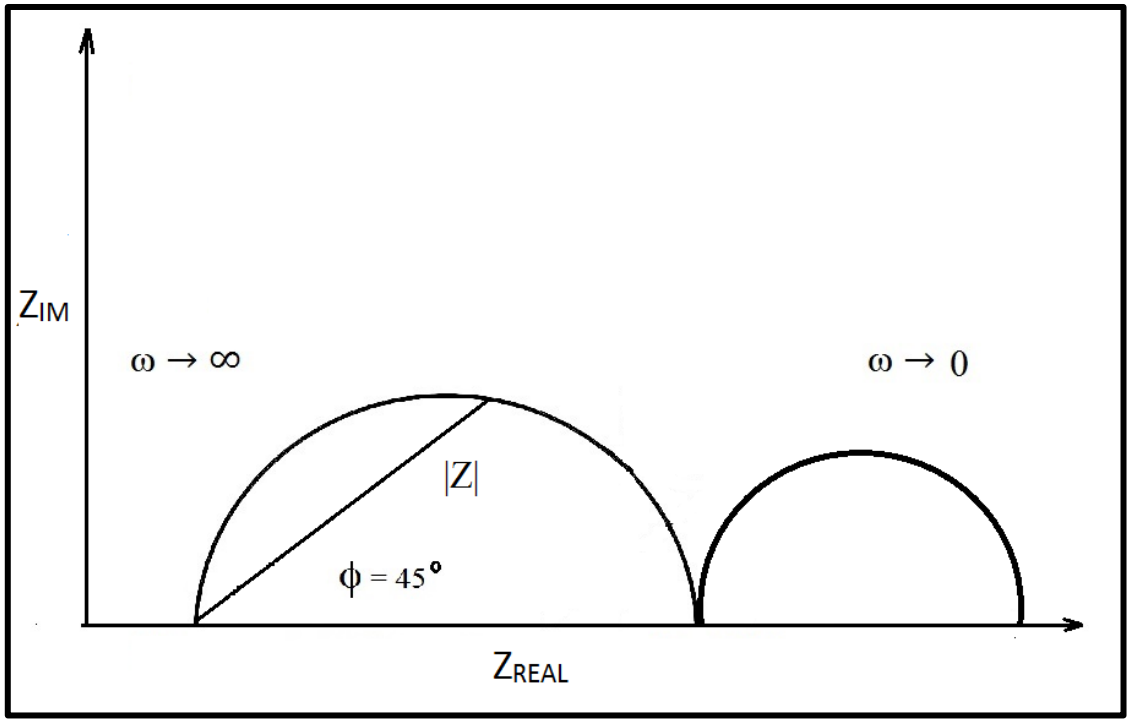

Figure 3.5 Nyquist plot for a Voigt Model where two semi-circles appear due to the system functioning as a multi-electrode system. The interface between this pocket of the solution and the bare metal is modeled as a double-layer capacitance in parallel with a kinetically controlled charge-transfer reaction.

as a double-layer capacitance in parallel with a kinetically controlled charge-transfer reaction

3.3 Relaxation Time Constant

Another critical parameter in the circuit is relaxation time $constant\ \tau = RC$, often referred as the "RC" time of the circuit. As has been described before, the interface has two distinct pathways, a capacitive storage path for the charges and a parallel reactive path for charge transfer. This is thus a parallel RC circuit. As discussed before in equation 6, for a

resistor (R) and a capacitor (C) circuit in parallel the equivalent Impedance is,

$$Z = R\frac{1+j\omega RC}{1+\omega^2R^2C^2} = R\frac{(1+j\frac{\omega}{\omega_O})}{(1+\frac{\omega^2}{\omega_O^2})} \quad \text{.....(3.7)}$$

where the relaxation frequency $\omega_o = 1/RC$. If $\omega_o >> \omega$ the circuit becomes open along the capacitor and the system becomes mass transfer controlled. Again, equation (7) can be written as

$$Z = R\frac{(\frac{\omega}{\omega_O})(\frac{\omega_O}{\omega}+j)}{(1+\frac{\omega^2}{\omega_O^2})} \quad \text{.....(3.8)}$$

Now if $\omega_o << \omega$, the circuit gets shorted and that refers to a kinetic-controlled phase. A higher RC time means allowing the system to store more charge and it exhibits capacitive nature while low RC time translates into resistive nature of the system as there is less storing of charge [92].

3.4 EIS in Microfluidic Device

In a microfluidic device, electrochemical changes occur at the electrodes on the application of an electrical field (AC voltage). Variations in the property of the electrolytes near the electrodes can be both resistive and capacitive [78]. The changes translate into impedance changes which can be represented as an equivalent electrical circuit model with common electrical components such as resistors, capacitors, and inductors [36]. In the last few decades, EIS has been used extensively in biochemical and medical applications, as it has proven to be a sensitive technique to detect and measure various biochemical or

biological events [5]. For example, it can be used for sensing the formation of antigen–antibody complexes, immune-sensing, DNA characterization and detection of DNA hybridization, as well as characterizing living cells, both quantitatively and qualitatively [5, 9, 11, 35, 36]. Thus, the EIS technique, combined with microfluidics, micromachining, and MEMS techniques, is a very useful and valuable tool in biosensors for easy and fast characterization of bio-samples [15]. Further, there are numerous studies in the literature that use EIS to measure the dielectric properties of cells, tissues and other biomolecules such as an antibody, antigen, and protein [11]. Unlike a typical cell colony average data, the differences between individual single cells have been evaluated by incorporating EIS with microfluidic devices. However, the chip dimensions for single-cell analysis needs to be of the length scale of individual cells [11]. The dielectric properties of biological cells reveal information about cell size, membrane resistance, membrane capacitance and cytoplasmic conductivity [15]. The presence of subcellular components, such as vacuoles, can also potentially be detected using EIS.

Other previous studies include glass-based chips with either multiple separate Pd electrodes, or a set of interdigitated Indium-Tin-oxide electrodes with which chromaffin or E. coli cells were characterized or detected, respectively [15]. Microscale impedance-based techniques were also used in Si-based chips, not to characterize the cells per se but to detect the variations in the suspension's impedance caused by the release of ionic species by metabolizing cells [11]. Since diffusion of the molecules determines most of the bio- and chemical reactions to the adequate places, the short distances in a microfluidic device permit the rapid detection by reducing the diffusion times. Both the mass and heat transport are faster in a microsystem, allowing a quasi-equilibrium state for the biochemical processes [9]. A variety of

microstructures can be used for optimization of transport processes, like vortices, pillars, or herringbone. All these desired properties of microfluidic devices are favorable in many biological and medical applications [9]. The fact that the microfluidic device is fabricated in glass confers it some key advantages such as enabling EIS analysis in a wide range of frequency spectrum, transparency for ease of observation using standard and confocal microscope, and hydrophilicity of the microfluidic channel. This latter feature is of particular importance as it causes self-driving capillary-based movement of the measured sample within the device to the measurement area [9].

3.5 Microelectrodes for Measuring EIS Spectra

Microelectrodes are miniaturized forms of bulk electrodes. Another type of electrodes, tubular flow electrodes, are infrequently used today as they are difficult to fabricate and integrate with flow devices [7]. As such, their utility would be greatly augmented by coupling with a versatile small-volume fluid handling system such as digital microelectrodes [93]. In literature, deviations from classical electrokinetics are seen as the sizes of the electrodes are reduced significantly [93]. Some of the interesting phenomena observed are, merging of the electrical double-layer and diffusion regimes, as well as enhanced fluid density and viscosity effects in the double-layer region [9]. It is worthwhile to mention that significant efforts have been made to fabricate microelectrodes To obtain highly sensitive detection, numerous fabrication approaches have been developed to construct metal nanostructures, such as electrochemical synthesis1, metal colloid preparation, nanoparticle self-assembly, E-beam lithography, vapor-liquid-solid (VLS) growth. Although these methods have synthesized nanostructures on a substrate with

high scattering enhancement factor, most of them are not compatible with pre-fabricated micro-chip. So it is a great challenge to fabricate nanostructures selectively on target microelectrodes *in-situ* impedance measurement. Microelectrodes used for single-cell analysis require small size. However, the double-layer impedance of the microelectrode existing in the electrode-electrolyte interface is inversely proportional to the electrode surface area. Downsizing of the electrode will unavoidably increase its double-layer impedance and thus degrade the sensitivity of the impedance measurement19. Fabricating nanostructures on microelectrodes can enlarge the effective surface area and therefore enhance the sensitivity of the EIS measurement.

Microelectrodes have a better signal to noise ratio than macro electrodes. As the size of an electrode decreases, mass transport to the electrode increases and the signal will decrease due to decreased electrode area. However, the potential (IR) drop, along with the background currents, significantly decreases. Hence, comparing the signal to noise ratio, the noise reduces faster than the reduction in signal, leading to a significant improvement in signal to noise ratio for microelectrodes [94, 95]. In summary, using a microelectrode over a macro electrode leads to increased fidelity or signal to noise ratio. Further, an array of microelectrodes also has a higher signal to noise ratio than a single electrode of the same size[96]. This is because the capacitive current (overall noise) is proportional to the active area (sum of the area of individual electrodes), while the signal is proportional to the geometric area (area of the electrode array) [96]. Microelectrode arrays have equal geometric areas to microelectrodes of similar size, but reduced active areas, improving the signal to noise ratio. The microelectrode is often coated with nanomaterials, which results in increased surface area [96]. This increases electron transfer rates and creates more sites

for the deposition of molecular probes. Hence, microelectrodes are ideal for samples where low volumes are desirable owing to their high sensitivity [96].

Microelectrodes modified with carbon nanotubes (CNTs) are useful for detection sensors since the CNTs enhance sensitivity and have electrocatalytic effects. CNTs can be grown on carbon fiber microelectrodes (CFMEs), but the intrinsic electrochemical activity of carbon fibers makes evaluating the effect of CNT enhancement difficult[33]. Previous studies have successfully demonstrated the integration of individually addressable CNT microelectrode arrays, coupled with microelectronics and micro- fluidic systems, in bioassays to exemplify advantages of miniaturization and multiplex detection [20]. The following chapter discusses a similar CNT-based microfluidic system incorporated with microelectrodes for mAb purification, detection, and analysis.

CHAPTER 4

EXPERIMENTATION

In this chapter, the experimental protocols, results and discussion on the results are presented. The protocols discussed in details involve CNT oxidation, chip fabrication, running antibody solutions and discussion of the results. The departure in the EIS spectrum from batch to continuous is discussed in details. The Nyquist plots from the EIS data for CNT surface activation, antibody attachment, antibody wash-off and antibody purification is shown. The plots are discussed in details to look at the possible classical EIS equivalent circuits to fit the data. Finally, the classical circuits are considered in more details to examine as to why they do not fit the EIS data.

4.1 Chip Fabrication

Figure 2 illustrates the lab-on-a-chip device. It consists of three layers, a top and bottom interdigitated electrode array and a middle layer of Carbon Nanotubes. The channels are fabricated from a medical grade acrylic double sided pressure sensitive tapes from ARcare® (Tape No: 90445) having a total thickness of 200 µm (including tape and adhesive coating layers) with 50 µm thick polyester release liners [40]. The tapes are laser cut to a channel of dimensions 100µm X 100µm X 1 mm and sonicated to remove any laser aberrations. The release liner from one side is released and mounted onto a Transwell® membrane to create an open microfluidic device. The other release liner is then removed, and the laser cut channels sealed between the two interdigitated electrode glass slides. The interdigitated electrodes are thermally deposited electrodes of 25 nm gold (Au). 25 nm Au

is optically transparent with negligible electrical resistance. A 5 nm titanium (Ti) will bind Au to gold.

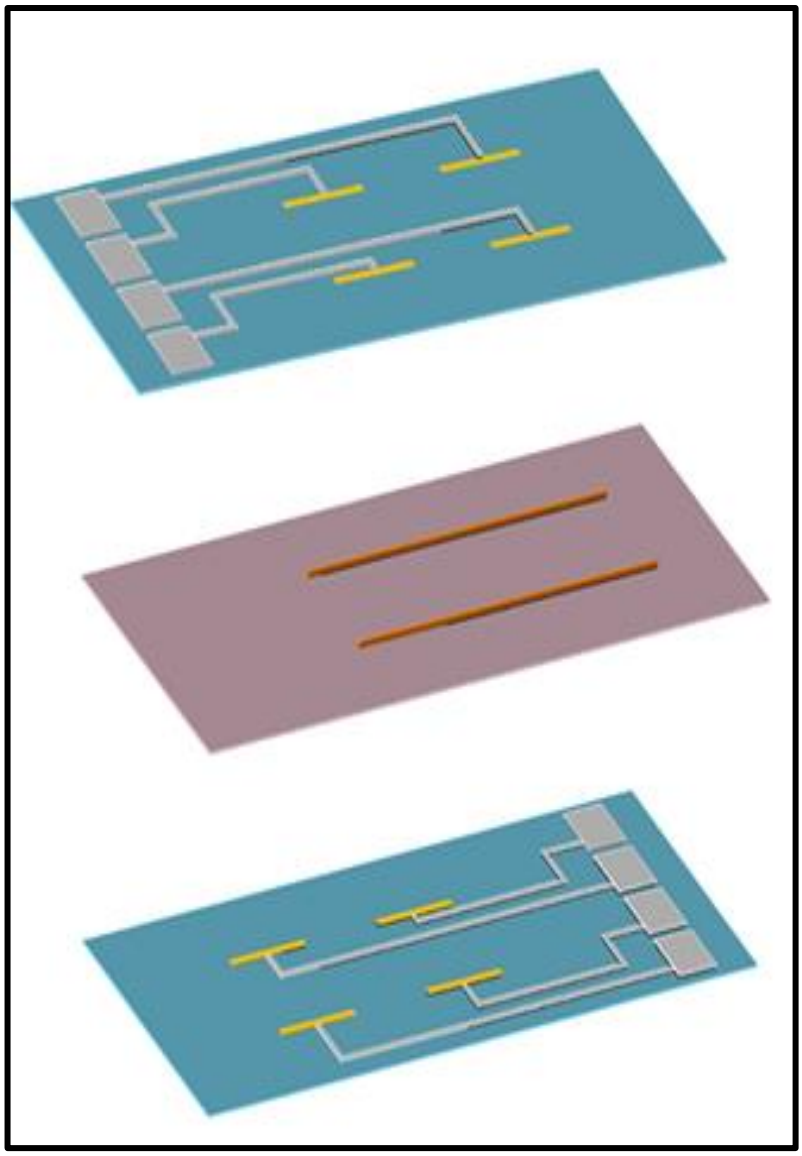

Figure 4.1 Layer 1 (glass slide), Layer 2 (adhesive) and Layer 3 (glass slide) oriented. Layer 1 has 4 square pads on the left-hand side, each connecting to an electrode array. Each square pad has a length of 5 mm and width of 5 mm. The electrode array has a length of 10 mm. In each electrode array, there are a parallel assembly of electrodes with a length of 500 µm and width of 10 µm with a distance of 30 µm between two electrodes

There had been a successful overcoming of challenges associated with the prevention of air bubble formation and leakage within the device. The interdigitation of the electrodes translates to a stronger electric field with amplified signal delivered by the Carbon Nanotubes. Upon connecting the device with an Electrical Impedance Spectroscopy (EIS) Machine, a DEP field is introduced to trap the CNTs within the channel. As seen in the above figure, the CNT solution will be introduced through the middle port. The

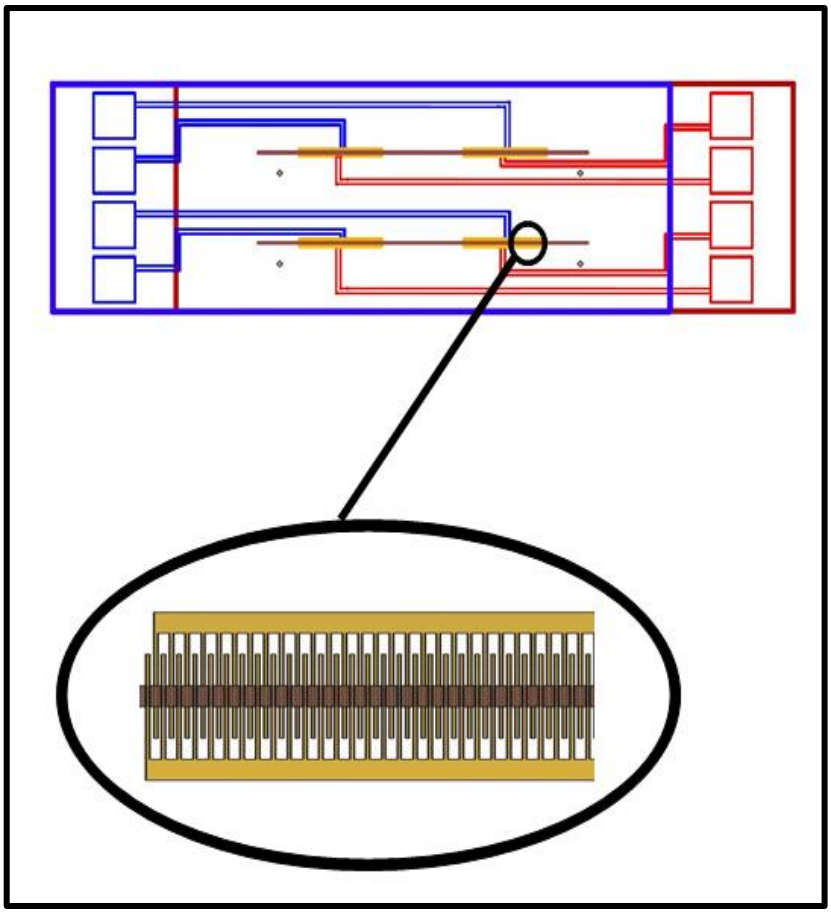

Figure 4.2 (A) Chip assembly and alignment **(B)** Close-up on interdigitated electrode array. The process of depositing Ti (5nm) and Au (25 nm) layer on glass slides involves soft lithography and e-beam. A 1 micron double sided tape with a 500-micron channel goes in between the two glass slide aligned in an interdigitated manner.

interdigitating of the electrodes provides the stronger electric field with amplified signal delivered by the CNTs. The flow splits into two halves and is discharged out of the other two ports. The electrochemical impedance spectroscopy (EIS) is measured using an array of microelectrodes of width 10 µm and length 500 µm, as microelectrodes have a better signal to noise ratio than macro electrodes.

As the size of an electrode decreases, mass transport to the electrode increases and the signal will decrease due to decreased electrode area. However, the power drop along with the background currents significantly decreases. Hence, comparing the signal to noise ratio, the noise reduces faster than the reduction in signal, leading to a significant improvement in signal to noise ratio for microelectrodes [94, 95]. Further, an array of microelectrodes has a higher signal to noise ratio than a single electrode of the same size. This is so because the capacitive currents (overall noise) is proportional to the active area (sum of the area of individual electrodes), while the signal is proportional to the geometric area (area of the electrode array) [96].

4.2 Carbon Nanotubes Oxidation

As a prelude to the attachment of mAb with CNTs, the CNTs have to be oxidized. The oxidation introduces a high density –COOH group into the nanotubes [86]. The protocol followed here is adapted from previous works that involved CNT oxidation in increasing the number of –COOH groups. The protocol involves digestion of 0.01 g of multi-walled CNT (length: 50 nm, diameter: 8 nm) in 10 ml 15 N HNO_3 at a temperature of 120° C for 24 hours. An in-house reflux condenser set-up was built in the chemical hood in the lab To ensure further reliability. Upon digestion, the CNTs are repeatedly centrifuged in DI water

for 5 minutes at 3000 rpm. The repeated centrifuging and washing is conducted until the supernatant approximates pH 7. [86] Once the desired pH level is achieved, CNTs are dried in vacuum.

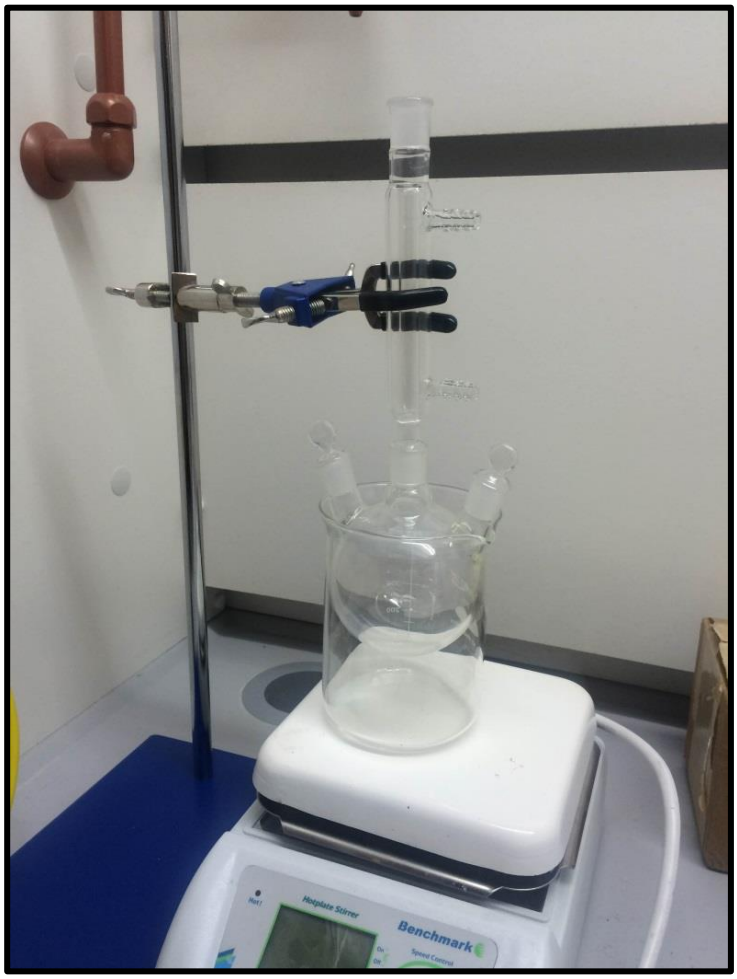

Figure 4.3 Experimental Set up for CNT oxidation that incorporates an in-house reflux condenser built in the chemical hood in the lab.

4.3 Carbon Nano Tube Loading in a Microfluidic Device

The CNT are loaded through one of the ports in the device. The device is connected to a function generator that applies a sinusoidal AC electric field with an RMS voltage of 10 V

peak to peak at 1 MHz across the interdigitated electrodes. The 10 V field translates to an electric field of about 10^4 V/cm across the interdigitated electrodes. The high field makes the CNT more conductive than 1X PBS, the solution in which the CNT is put in. The interdigitated electric field traps the CNT along the electric lines of forces[35]. This kind of trapping in high electric fields for conductive particles is called as positive dielectrophoretic force traps [20]. Such traps have been shown to trap biomolecules and colloids in many microfluidic designs [29, 78].

The interdigitation of the electrodes ensures that a component of the dielectric trapping force field always opposes the drag force from the fluid flow, keeping the CNT's trapped even under large shear forces (high flow rates). Thus the interdigitating of the electrodes

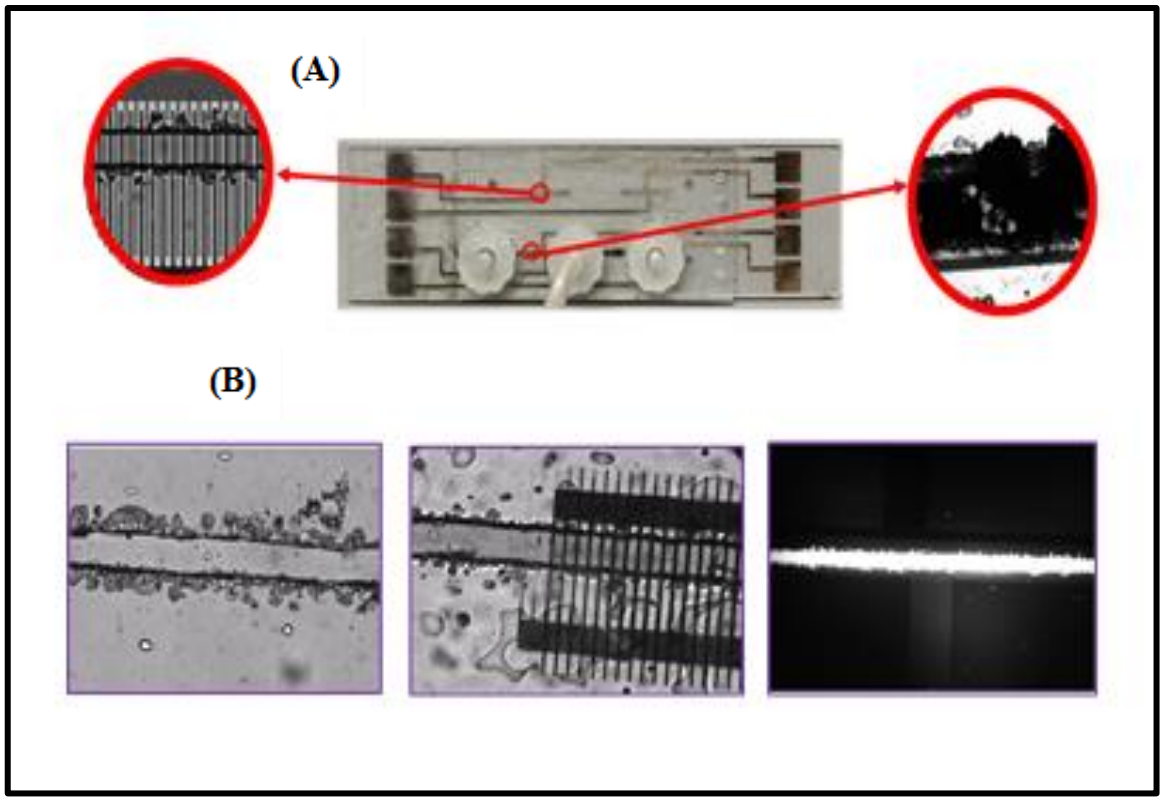

Figure 4.4 (A) Diagram of assembled chip with inset showing the placement of the interdigitated electrodes with CNT trapped. (B) Leak-proof flow of solution through the 500 um channel without any debris

translates to a stronger electric field that can trap the CNTs in the device under high shear force.

4.4 Monoclonal Antibody Attachment

The attachment of the mAbs to the CNTs was carried out monoclonal antibody attachment was conducted in both continuous and batch process. The detailed protocol for both the processes is described in details below.

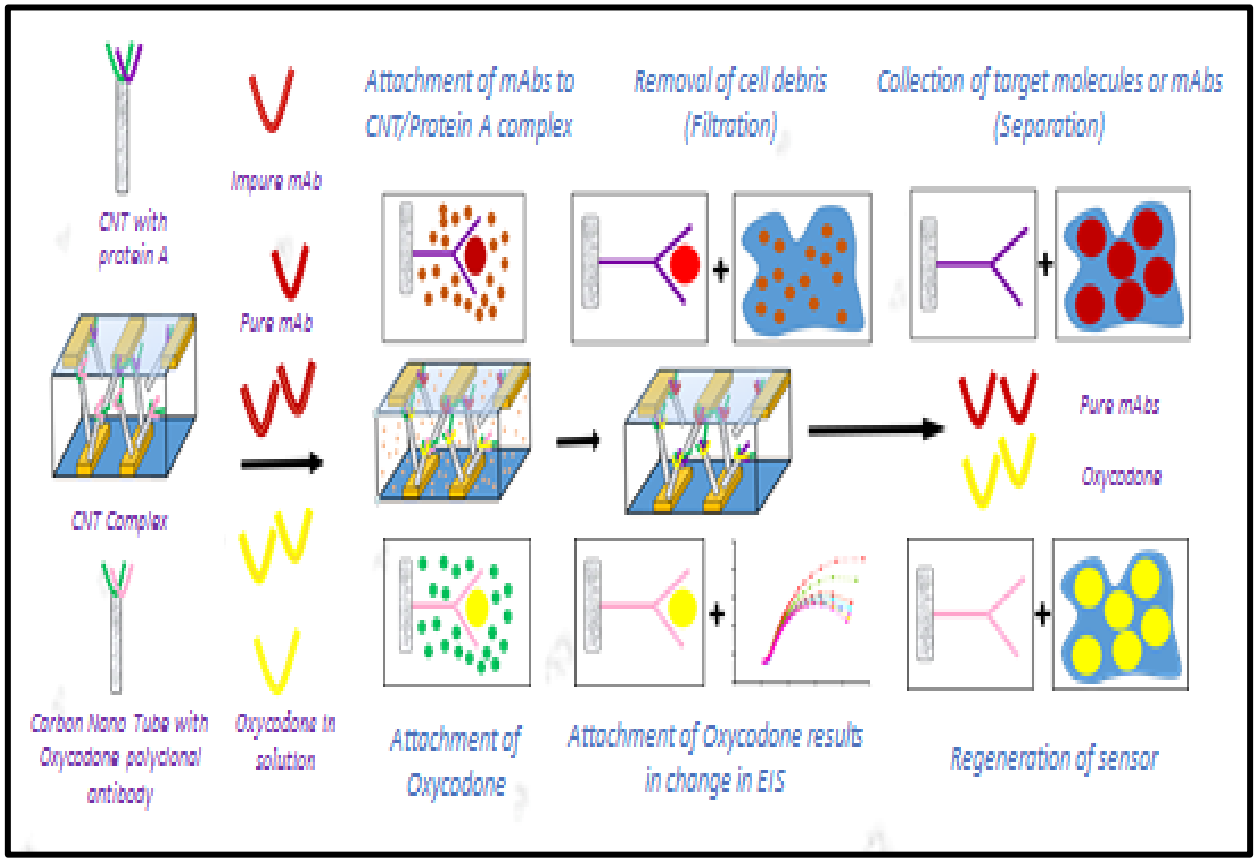

Figure 4.5 Experimental protocol for separation of monoclonal antibodies. The protocol has three distinct chemical engineering unit operations namely capture, filtration and separation/purification, all achieved on a single chip

4.4.1 Batch Process

A **batch process** is any manufacturing **process** that runs in short time bursts, where the quantity or scale of manufacture does not justify the continuous operation. Nearly all pharmaceutical production is done in **batches.** The motivation to design chemical processes into miniaturized, integrated fluidic devices stems from the advantages gained in efficiency by automation and parallelization, reduction in errors, high throughput, minimization of chemical usage, and portability of chemical analysis equipment to the point of use. Here, we ran our monoclonal antibody protocol in a batch process. The well showed in **figure 4.6** was constructed around one of the electrodes on the glass slide. EIS

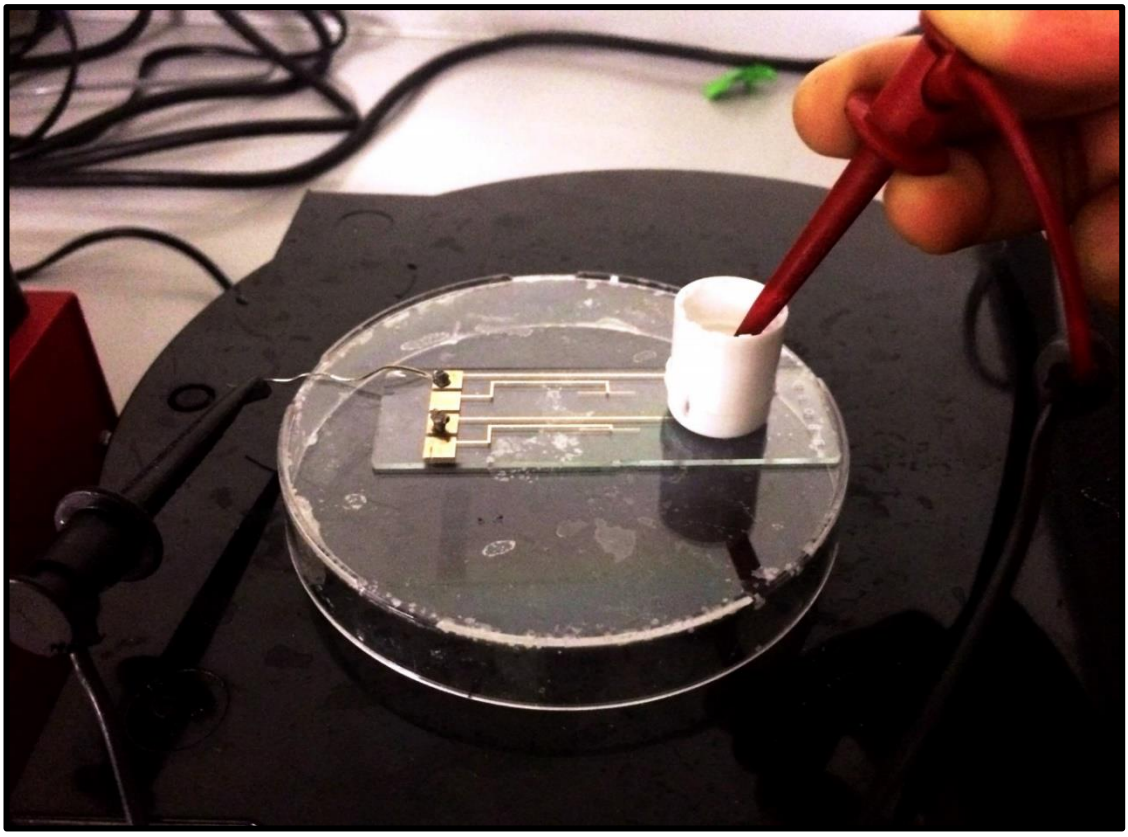

Figure 4.6 Experimental run for attachment of Anti Oxycodone mouse monoclonal antibody to functionalized CNT (in green) followed by Anti-mouse goat polyclonal antibody in a batch process with 0.1x PBS solution

data was obtained for CNT in 0.1x PBS solution followed by NHS-EDAC, monoclonal and polyclonal antibodies respectively. As the results from batch studies of EIS is well documented in the literature, we wanted a point of comparison with our continuous process as has been done elsewhere [20].

4.4.2 Continuous Process

The first step in the continuous process in the preparation of the immunoassay is the attachment of monoclonal antibodies to the CNT platform by performing NHS-EDAC

Figure 4.7 Experimental run for attachment of Anti Oxycodone mouse monoclonal antibody to functionalized CNT (in green) followed by Anti-mouse goat polyclonal antibody in a continuous process with 0.1x PBS solution

chemistry as shown in **figure 4.7**. NHS (0.4 mg/ml) and EDC (0.6mg/ml) are mixed in 5:2 ratios and is charged at 2 µl/min over the CNTs inside the device. The –COOH group in

the CNTs tend to activate within an hour after the NHS-EDC charge into the device. Next, 1 nM Anti-oxycodone mouse monoclonal antibody (from Abcam) is charged at 2 µl/min and further shifts in the Nyquist plot is observed in the corresponding EIS data (**figure 4.9**). The frequency measurement was taken from 100 MHz to 1 kHz with an applied AC voltage of 1 V using a 4294A Agilent EIS machine.

However, the curvature of the Warburg element is not clear and more studies need to be performed (as detailed in aim 2). Finally, secondary 1 nM anti-mouse goat polyclonal antibody specific to the Anti-oxycodone mouse monoclonal antibody is charged into the system at 2 µl/min. The chip is then washed in PBS for an hour at 5 µl/min to knock off the secondary antibodies to see whether the chip comes back to the original signal. All the flow rates were kept constant at 5ul/min. Moreover, for all the charges the buffer used was 0.1x PBS with a pH of 7.5.

4.4.3 Polyclonal Antibody Attachment

Another set of on-chip experiment was run for Anti-mouse goat polyclonal antibody. The first step in the preparation of the immunoassay is as same as the attachment of monoclonal antibodies to the Carbon Nanotube platform by performing NHS-EDAC chemistry as described in section 4.4.1. Again, NHS (0.4 mg/ml) and EDC (0.6mg/ml) was mixed in 5:2 ratios and was charged over the functionalized CNTs inside the device for surface activation. The –COOH group in the CNTs tend to activate within an hour after the NHS-EDC charge into the device. EIS reading had been taken for CNT in PBS followed by NHS-EDC charge. Afterward, the EIS data for polyclonal antibody has been obtained. All

the flow rates were kept constant at 5ul/min. Moreover, for all the charges the buffer used was 0.1x PBS with a P_H of 7.5

4.6 Results and Discussion

The observed EIS spectrum (Nyquist curve) in **figure 4.8** reflects the change in CNTs to macromolecule passage including surface activation in a batch process. There are no significant shifts of the Nyquist diagram when NHS-EDC is charged into the system or from the addition of polyclonal/monoclonal antibodies as has been observed elsewhere [20]. However, in the continuous processed **(figure 4.9 - 4.11)**, a significant change is observed on the addition of NHS-EDC and adding antibodies. The Plots for CNT in 0.1x PBS and NHS-EDC do not overlap on top of each other. *It is worthwhile to mention here that this is a first instance of carrying out EDC chemistry on a chip, where a measurable change in EIS signal has been observed (**figure 4.9**).* The addition of primary antibody (mAb) to the CNT platform results in a shift in the electrical impedance that occurs as a result of binding of the primary antibody to the CNT surface. Finally, also on the addition of secondary 1 nM anti-mouse goat polyclonal antibody specific to the Anti-oxycodone mouse monoclonal antibody to the system at 2 µl/min, the EIS data changes significantly as observed in **figure 4.9**. As can be seen in **figure 4.9**, on washing with PBS for an hour, the EIS comes back to the original level. This in indicated by the mixed color of the first line in the graph plotted in Origin as both the red curve and the green curve superimpose. It is worthwhile to note that the PBS solution is washing out the loosely bound secondary antibodies from the primary monoclonal antibodies due to the extensive shear in the device.

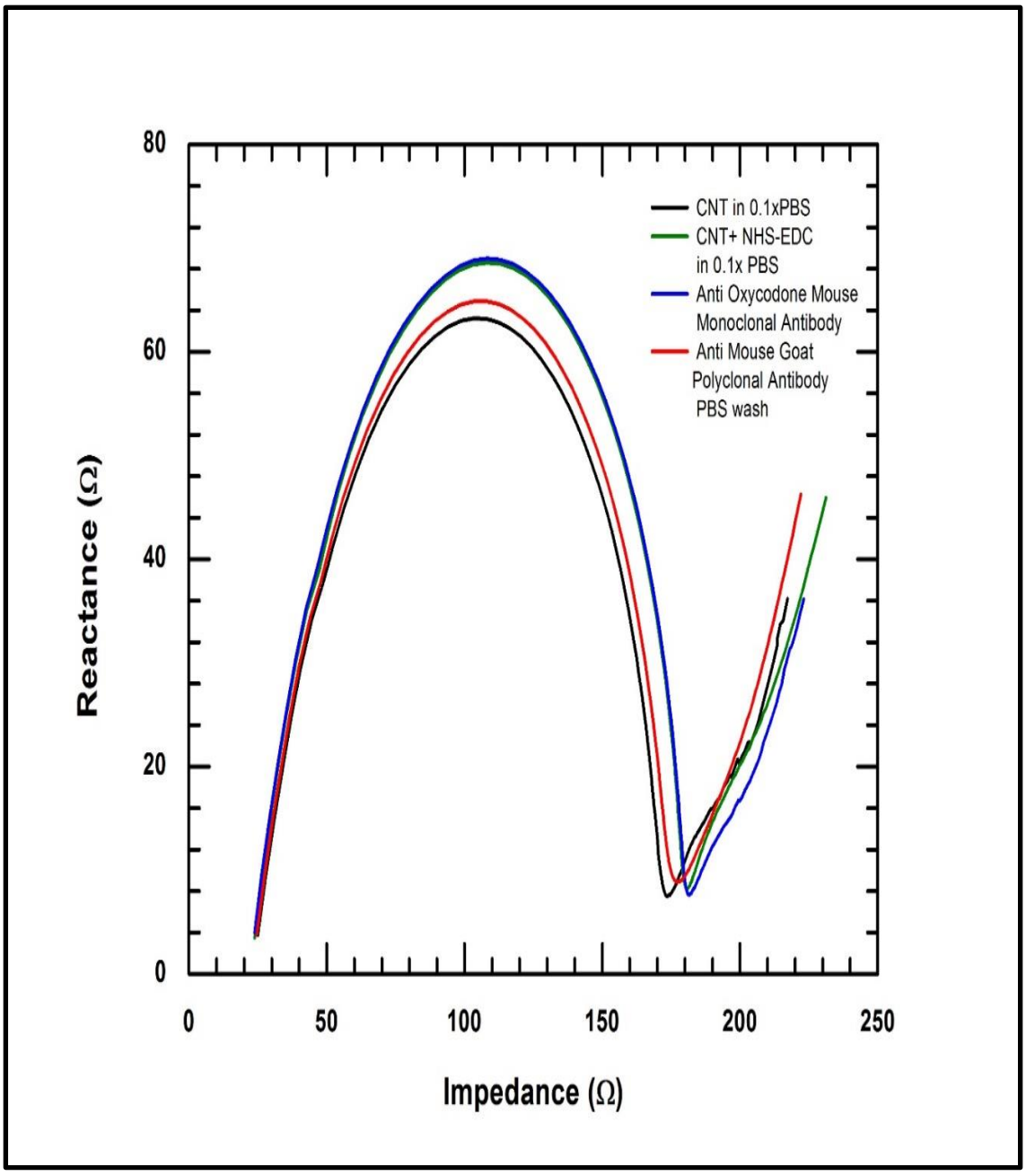

Figure 4.8 A schematic illustration of impedance spectra in the form of Nyquist plots for a batch process, a) Carbon Nanotube in 0.1x PBS, whose impedance is controlled by the diffusion of to the and from the electrode surface (in blue) b) Surface activation by EDC-NHS exhibiting a slight change in impedance (in blue) c) Attachment of Anti Oxycodone mouse monoclonal antibody to functionalized CNT (in green) d) Attachment of Anti-mouse goat polyclonal antibody with monoclonal antibody exhibiting little shift in impedance and Warburg.

Figure 4.9 depicts the schematic representation of open flow CNT platform with the channel inset to show different zones and the electrode arrangements. In electrochemical studies of biomolecules by impedance measurements, the electronic and ionic currents around the electrode surface are governed by the Randle circuit. The circuit has a capacitance (CPEe) which is in series with diffusional Warburg Resistor (WS1). Re is the intrinsic resistance in the circuit while Le is the parasitic inductor in the circuit due to noises (see figure 4.12) [5]. It is well established that at lower frequencies, the current is resistive. At higher frequencies, the double layer capacitor (CPEe) dominates [5]. The EIS shift clearly indicated that the charge transfer resistance or R1 is decreasing from bare CNT to EDC activated CNT to monoclonal antibodies and increases on the addition of secondary antibodies). Interfacial charge transfer resistance (R1) which is in parallel with a double layer

It is worthwhile to bear in mind the two competing phenomenon here. Firstly, CNTs, as they are touching the electrodes on the glass surface, behave as extended electrodes here. Secondly, the addition of more charge to the CNT surface from bare CNT to EDC-CNT to antibody functionalized CNT (OCab-CNT), decreases R1. On the other hand with the addition of the pAb antibody molecules, the electrode surface area of the CNT visible to the electrolyte decreases, leading to a decrease in R1. Initially, the addition of charge dominates (decrease in R1) while on the addition of the secondary antibodies, R1 increases due to the decreasing CNT surface area. Unlike the monoclonal runs, upon polyclonal antibody charge right after EDC-NHS the plot shifts toward right denoting an increase in impedance, which was not the case regarding monoclonal antibodies. Such behaviors can

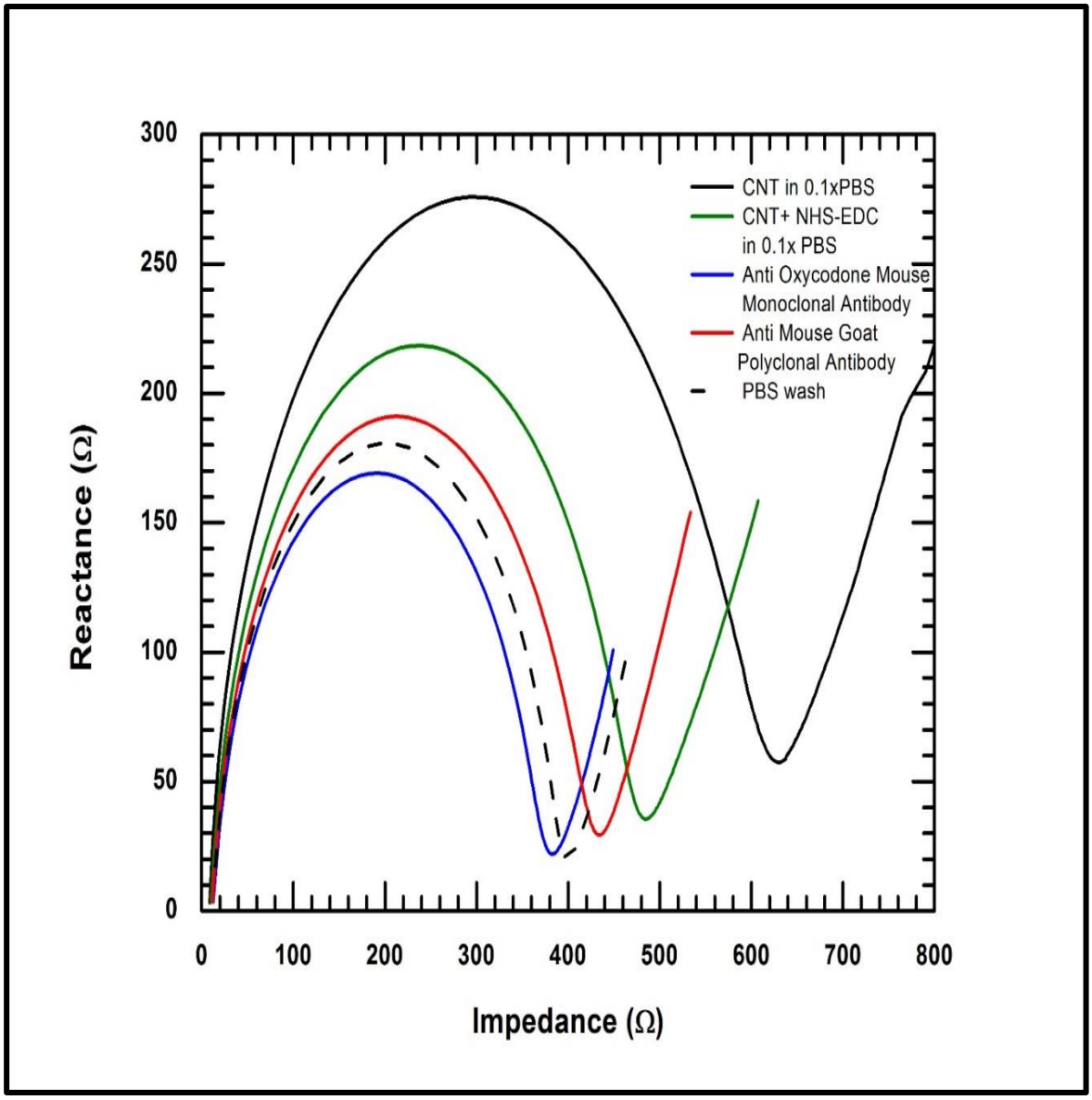

Figure 4.9 A schematic illustration of impedance spectra in the form of Nyquist plots for a) Carbon Nanotube in 0.1x PBS, whose impedance is controlled by the diffusion to the and from the electrode surface (in black) b) Surface activation by EDC-NHS exhibiting a significant rise in impedance accompanied by a pronounced Warburg (in blue) c) Attachment of Anti Oxycodone mouse monoclonal antibody to functionalized CNTs (in green) with further shift in impedance and Warburg d) Attachment of Anti-mouse goat polyclonal antibody to monoclonal antibody with significant change in impedance and Warburg (in red). e) PBS wash after 160 minutes that approximates the plot for monoclonal antibody attachment to functionalized CNTs.

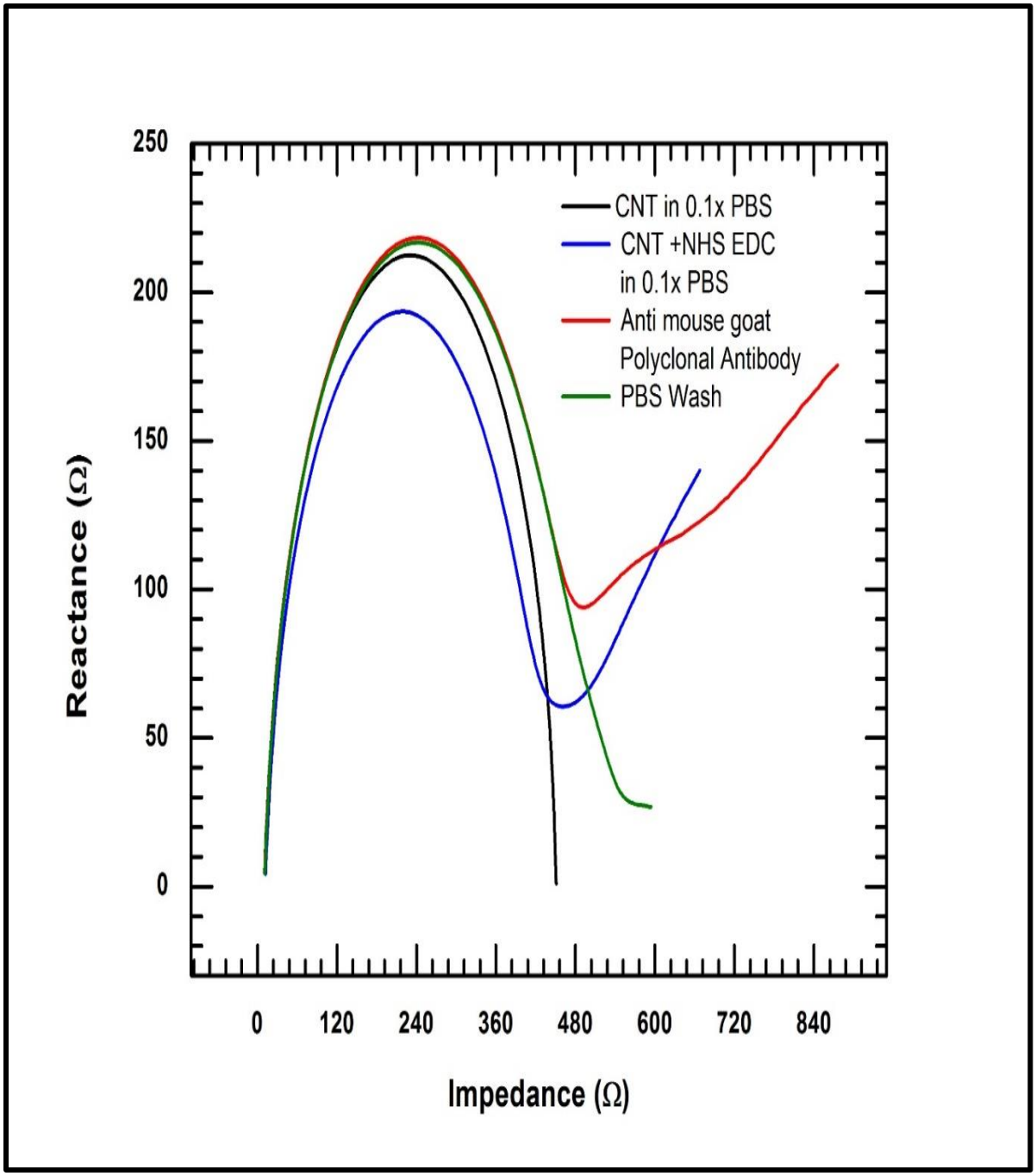

Figure 4.10 A schematic illustration of impedance spectra in the form of Nyquist plots for a) Carbon Nanotube in 0.1x PBS, whose impedance is controlled by the diffusion to the and from the electrode surface (in black) b) Surface activation by EDC-NHS exhibiting a significant rise in impedance accompanied by a pronounced Warburg (in blue) c) Attachment of Anti-mouse polyclonal antibody to functionalized CNTs (in red) with further shift in impedance and Warburg d) PBS wash after 160 minutes

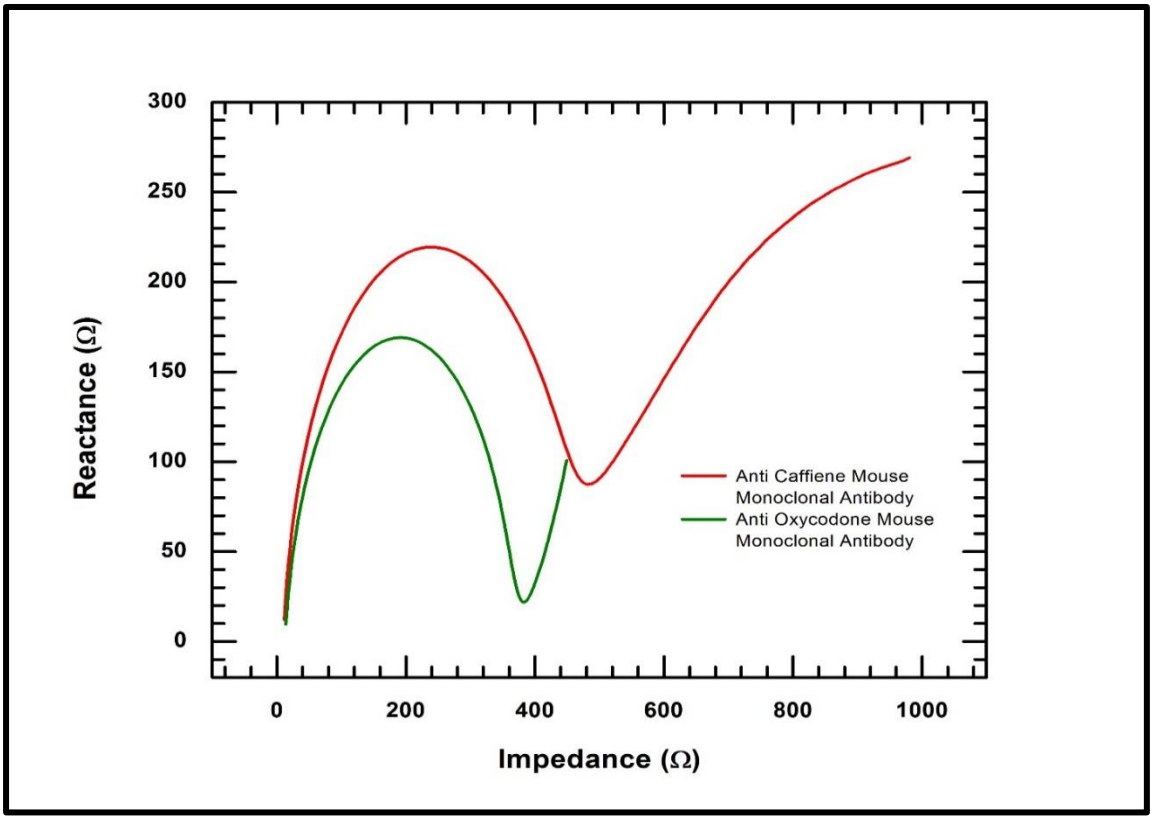

Figure 4.11 A schematic illustration of impedance spectra in the form of Nyquist plots for a) Attachment of Anti Oxycodone mouse monoclonal antibody with functionalized CNTs upon performing NHS-EDC chemistry (in green) b) Attachment of Anti-caffeine mouse monoclonal antibody to functionalized CNT. Both the antibodies exhibit prominent Warburg with a significant difference in their respective impedance based on their structures.

monoclonal and Anti-caffeine mouse monoclonal antibody to functionalized CNT has been compared in the following Nyquist diagram. Both the antibodies exhibit prominent Warburg with a significant difference in their respective impedance based on their structures. The Anti Oxycodone mouse monoclonal demonstrates a steeper Warburg than that of the Anti-caffeine mouse monoclonal antibody. The steeper Warburg indicates a more capacitive process. This is due to the higher charge in the anti oxycodone antibody in comparison to the anti-caffeine antibody. From the figure, it can also be assumed that

Anti Oxycodone mouse monoclonal is more conductive than Anti-caffeine mouse monoclonal antibody.

4.7 Data Fitting

Initial fitting of the data using a commercial EIS software Zview® from Scribner Associates gave us good fits. However, it could not fit the Warburg Resistor very well as can be seen in **figure 4.12 (B)**. The fitting is poor, specifically, at lower frequencies when diffusion dominates, We believe that this is due to the incorrect boundary condition assumed in classical derivations of the Warburg resistance. However, the closed packing of the CNT can give rise to other resistances, including a possible convective resistance term (which has not been described before). This departure from classical formulations can be ascribed to the structure of the CNT inside the channel. Here, the CNT exists as nanostructured CNT wherein the ionic flux is confined in local nanodomains. Hence the boundary condition for the diffusion equation needs to be suitably modified into a mixed Robbin boundary condition. Further, the boundary condition as it depends on the nanostructured CNT surface, the antibody structure with its orientation of the charged groups can modify the ionic flux equation. This modification in the EIS spectra is seen in Figure where depending on the antibody moiety; different antibodies give rise to different Warburg signals.Hence, the Warburg element in the equivalent circuit can be modeled from first principles to represent the structure of the antibody primarily looking at the orientation of the charged molecules. The model will be verified by using different concentrations of mAbs and secondary antibodies. It is worthwhile to note that any correlations developed here would

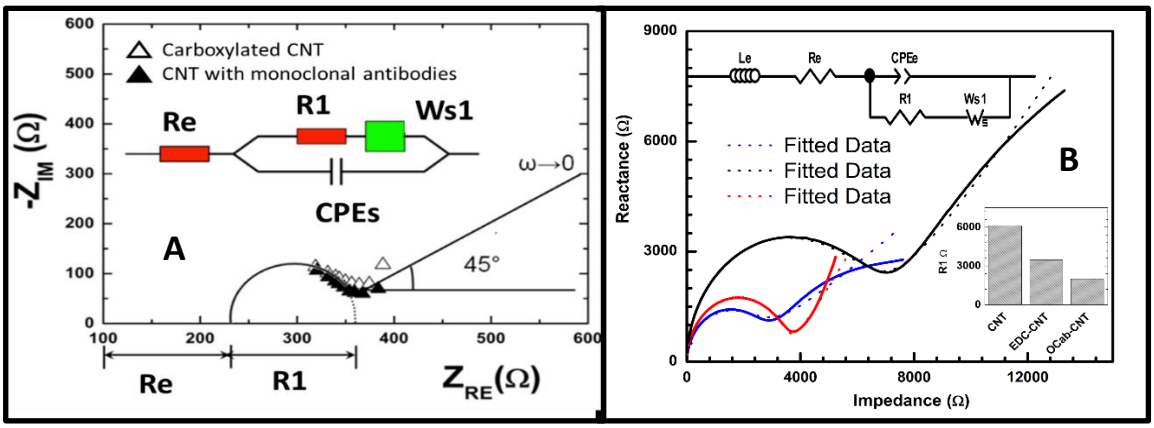

Figure 4.12 (A) Graphical presentation of the Nyquist diagram for a Randle circuit with an inset schematic of the circuit. Typical batch Nyquist plots are shown for bare CNT and CNT with mAbs in 1X PBS buffer in an applied AC field of 1 V at a frequency of 100 MHz to 1KHz. Extrapolation to obtain R1 is not possible due to the loop double-layer impedance signature. In fact, both bare and CNT with mAbs are indistinguishable at the important high-frequency end of the Warburg branch. **(B)** Fitting of the EIS signal from the running of the primary antibodies, NHS-EDC and bare CNT using Zview® Software. Clearly the fit is good at the higher frequencies which shows that the circuit model works at the higher frequency. However, the fit is poor at the lower frequencies which indicate that the classical diffusive Warburg element is wrongly described.

be averaged correlations and not for single mAbs. Further, the EIS results need to be also modeled and how the circuit elements in the equivalent circuit correlate to changes in ionic strength, pH, flow rate (changing shear).

CHAPTER 5

CONCLUSION

AND FUTURE WORK

5.1 Future Work

Raman spectroscopy is a powerful technique for solid-state in situ protein pharmaceutical analysis within glass containers or for separate samples [97]. The penetration of visible laser light through glass enables in-situ analysis to be performed without any sample manipulation [97]. The characteristic fingerprint feature of Raman spectra for proteins allows differentiation between protein product and placebo and between different protein products. Our system involves label-free non-invasive detection. A Raman analysis can be performed on the antibodies to ensure further reliability. Near-infrared Raman spectroscopy (NIRS) has gained increasing prominence as a tool for quantitative analysis of IgG and IgM antibodies[98]**.** It can also perform the analysis of thermal stability of the antibodies at various concentrations and helps distinguish unfolding from aggregation events. The Raman scattering technique is a vibrational molecular spectroscopy which, derives from an inelastic light scattering process. In our study, the analysis of mAbs structure can be performed with Raman spectroscopy, where a laser photon is scattered by the antibody and it loses (or gains) energy during the process [99]. The amount of energy lost is seen as a change in energy (wavelength) of the irradiating photon. This energy loss is characteristic for a particular bond in the molecule. The Raman signal produces a precise spectral sample fingerprint, unique to each atom, a group of atoms or individual molecule. Also for the following reason Raman proves to be the most efficient method for the chemical and structural analysis of out antibodies [100]:

(i) Raman can be used to analyze in aqueous solutions,

(ii) The intensity of spectral features is directly proportional to the concentration of the particular species,

(iii) Raman requires little or no sample preparation, and

(iv) The use of a Raman microscope provides very high level of spatial resolution and depth discrimination.

Our microfluidic device proves to be an effective tool for qualitative analysis. However, challenges exist for using the chip for quantitative analysis. The replacement of a CNT-binding platform by ZnO will be done to approach from a quantitative analytical point of view, ZnO is an n-type direct bandgap semiconductor with a large exciton binding energy of 60 meV and Eg of 3.37 eV at room temperature[101]. Hence, it is regarded as a promising photonic material with near-ultraviolet (near-UV) emission, electric conductivity, piezoelectricity and optical transparency [102]. Using a solid–vapor phase thermal sublimation technique, nano comes, nanorings, nano-helixes/nano-springs, nanobelts, nanowires and nanocages of ZnO have been synthesized under specific growth conditions [103]. For our work, the vertical well-aligned ZnO Nanowire arrays can be prepared on glass templates where ZnO seed layers can be grown on glass via radio-frequency sputter deposition. This shall pave the way for quantitative analysis through our device as the amount of ZnO nanowire is known once grown on the chip.

5.2 Conclusion

The significance of the proposed work is in the development of a new shear enhanced platform with real-time spectroscopic observation tools to study and purify monoclonal

antibodies. The lab-on-a-chip device will be used as a generic platform and can be interfaced with other drug manufacturing instruments for the rapid production of "on-demand" drugs. Although a considerable amount of literature exists related to the construction of complex chromatographic techniques for the continuous production of mAbs, development of a simple, robust, high yield, large mAb capture ratio from cell culture fluid is nonexistent to date. This rapid, cost-effective, highly sensitive and selective microfluidic platform will use enhanced shear force to purify mAbs. Simultaneously, the interdigitated electrodes will use EIS to measure the binding event and strength (affinity testing) of mAbs to the antigen, allowing for an antigen microarray/ELISA from the same platform. Till now, there is no literature for shear studies of monoclonal antibodies. The critical questions asked here will be, whether the shear force can degrade the efficiency and affinity of the mAb, how do pH and ionic strength in conjugation with shear affect mAb efficiency and affinity. This is critical for optimization of flow based systems for manufacturing drugs as rapid continuous manufacturing becomes more and more commonplace. This will be accomplished by using multiple lab-on-a-chip devices simultaneously to do kinetic assay testing, and specificity tests on the chip. This device should outperform traditional systems both in their portability, yield, and capture efficiency. The packing of the CNT inside the microchannel should have unprecedented high surface to volume areas, high and sensitive electrical signal, and customizable surface chemistries, and therefore serve as an ideal platform to build novel mAb analysis systems.

REFERENCE

Whitesides, G.M., *The origins and the future of microfluidics.* Nature, 2006. **44**(27): p. 368-373.

Chiou, C.-H. and G.-B. Lee, *Minimal dead-volume connectors for microfluidics using PDMS casting techniques.* Journal of Micromechanics and Microengineering, 2004. **14**(11): p. 346-353.

Mark, D., et al., *Microfluidic lab-on-a-chip platforms: requirements, characteristics and applications.* The Royal Society of Chemistry 2010. **39**(11): p. 1153-1182.

Ying, Y.-L., et al., *Nanopore Biosensors: Monitoring of an ATP-Binding Aptamer and its Conformational Changes Using an α-Hemolysin Nanopore (Small 1/2011).* Small, 2011. **7**(1): p. 1-1.

El-Safty, S.A., et al., *Nanofiltration: Building-Block-Based Mosaic Cage Silica Nanotubes for Molecular Transport and Separation (Small 1/2011).* Small, 2011. **7**(1): p. 2-2.

Wang, J., et al., *Simultaneous Detection of Copper, Lead and Zinc on Tin Film/Gold Nanoparticles/Gold Microelectrode by Square Wave Stripping Voltammetry.* Electroanalysis, 2012. **24**(8): p. 1783-1790.

Fritsch-Faules, I. and L.R. Faulkner, *Use of microelectrode arrays to determine concentration profiles of redox centers in polymer films.* Analytical Chemistry, 1992. **64**(10): p. 1118-1127.

Ishige, Y., et al., *Feasibility Study on Direct Counting of Viruses and Bacteria by Using Microelectrode Array.* Electroanalysis, 2012. **24**(1): p. 131-139.

Weber, S.G., *Signal-to-noise ratio in microelectrode-array-based electrochemical detectors.* Analytical Chemistry, 1989. **61**(4): p. 295-302.

Nguyen, B.T.T., et al., *Electrochemical impedance spectroscopy characterization of nanoporous alumina dengue virus biosensor.* Bioelectrochemistry, 2012. **88**: p. 15-21.

Han, L., et al., *A Label-Free Electrochemical Impedance Cytosensor Based on Specific Peptide-Fused Phage Selected from Landscape Phage Library.* Scientific Reports, 2016. **6**: p. 22199.

Jüttner, K., *Electrochemical impedance spectroscopy (EIS) of corrosion processes on inhomogeneous surfaces.* Electrochimica Acta, 1990. **35**(10): p. 1501-1508.

Johnson, B.J., et al., *Electrochemical impedance spectroscopy studies of lithium diffusion in doped manganese oxide.* Journal of Power Sources, 1997. **68**(2): p. 634-636.

Resch-Genger, U., et al., *Quantum dots versus organic dyes as fluorescent labels.* Nat Meth, 2008. **5**(9): p. 763-775.

Hu, C., et al., *Improved EIS Performance of an Electrochemical Cytosensor Using Three-Dimensional Architecture Au@BSA as Sensing Layer.* Analytical Chemistry, 2013. **85**(10): p. 5200-5206.

Wiedemann, D.J., et al., *Strategies for low detection limit measurements with cyclic voltammetry.* Analytical Chemistry, 1991. **63**(24): p. 2965-2970.

Weber, S.G. and J.T. Long, *Detection Limits and Selectivity in Electrochemical Detectors.* Analytical Chemistry, 1988. **60**(15): p. 903A-913A.

Daniels, J.S. and N. Pourmand, *Label-Free Impedance Biosensors: Opportunities and Challenges.* Electroanalysis, 2007. **19**(12): p. 1239-1257.

Curioni, M., et al., *Correlation between electrochemical impedance measurements and corrosion rate of magnesium investigated by real-time hydrogen measurement and optical imaging.* Electrochimica Acta, 2015. **166**: p. 372-384.

Basuray, S., et al., *Shear and AC Field Enhanced Carbon Nanotube Impedance Assay for Rapid, Sensitive, and Mismatch-Discriminating DNA Hybridization.* ACS Nano, 2009. **3**(7): p. 1823-30.

Zhang, Z., et al., *All-carbon sp-sp(2) hybrid structures: Geometrical properties, current rectification, and current amplification.* Scientific Reports, 2013. **3**: p. 2575.

Wu, J.-x., S.-e. Zhang, and X.-p. Zhou, *Monoclonal antibody-based ELISA and colloidal gold-based immunochromatographic assay for streptomycin residue detection in milk and swine urine.* Journal of Zhejiang University. Science. B, 2010. **11**(1): p. 52-60.

Sushma Drabu, et al., *Carbon Nanotubes in Pharmaceutical Nanotechnology: An introduction to Future Drug Delivery System.* Journal of Chemical and Pharmaceutical Research, 2010. **2** (1): p. 444-457.

Neill, A., et al., *Characterization of Recombinant Monoclonal Antibody Charge Variants Using OFFGEL Fractionation, Weak Anion Exchange Chromatography, and Mass Spectrometry.* Anal Chem, 2015. **87**(12): p. 6204-11.

Lowder, J.N. and R. Levy, *Monoclonal Antibodies—Therapeutic and Diagnostic Uses in Malignancy.* Western Journal of Medicine, 1985. **143**(6): p. 810-818.

Goodall, M., *Mouse Monoclonal Antibodies*, in *Animal Cell Biotechnology: Methods and Protocols*, N. Jenkins, Editor. 1999, Humana Press: Totowa, NJ. p. 73-98.

Finnis, C.J.A., et al., *High-level production of animal-free recombinant transferrin from saccharomyces cerevisiae.* Microbial Cell Factories, 2010. **9**: p. 87-87.

Kuhlmann, W.D., *Purification of antibodies by the use of biochemical and immunochemical techniques* 2008.

Senapati, S., et al., *A nanomembrane-based nucleic acid sensing platform for portable diagnostics.* Top Curr Chem, 2011. **304**: p. 153-69.

Swartz, M., *HPLC DETECTORS: A BRIEF REVIEW.* Journal of Liquid Chromatography & Related Technologies, 2010. **33**(9-12): p. 1130-1150.

Guimarães Sá Correia, M., et al., *Microfluidic manufacturing of phospholipid nanoparticles: Stability, encapsulation efficacy, and drug release.* International Journal of Pharmaceutics, 2017. **516**(1–2): p. 91-99.

Herranz-Blanco, B., et al., *Microfluidics platform for glass capillaries and its application in droplet and nanoparticle fabrication.* International Journal of Pharmaceutics, 2017. **516**(1–2): p. 100-105.

Basuray, S. and H.C. Chang, *Induced dipoles and dielectrophoresis of nanocolloids in electrolytes.* Phys Rev E Stat Nonlin Soft Matter Phys, 2007. **75**(6 Pt 1): p. 060501.

Basuray, S. and H.C. Chang, *Designing a sensitive and quantifiable nanocolloid assay with dielectrophoretic crossover frequencies.* Biomicrofluidics, 2010. **4**(1): p. 13205.

Basuray, S., H.H. Wei, and H.C. Chang, *Dynamic double layer effects on ac-induced dipoles of dielectric nanocolloids.* Biomicrofluidics, 2010. **4**(2).

Mavrogiannis, N., et al., *Monitoring microfluidic interfacial flows using impedance spectroscopy.* Sensors and Actuators B: Chemical, 2017. **239**: p. 218-225.

Lee, J., et al., *Protein fouling in carbon nanotubes enhanced ultrafiltration membrane: Fouling mechanism as a function of pH and ionic strength.* Separation and Purification Technology.

Umemura, K., et al., *Non-uniform binding of single-stranded DNA binding proteins to hybrids of single-stranded DNA and single-walled carbon nanotubes observed by atomic force microscopy in air and in liquid.* Applied Surface Science, 2016. **388, Part A**: p. 381-384.

Paul, K.B., et al., *One step biofunctionalized electrospun multiwalled carbon nanotubes embedded zinc oxide nanowire interface for highly sensitive detection of carcinoma antigen-125.* Biosensors and Bioelectronics, 2017. **88**: p. 144-152.

Fang, S., et al., *A label-free multi-functionalized electrochemical aptasensor based on a Fe3O4@3D-rGO@plasma-polymerized (4-vinyl pyridine) nanocomposite for the sensitive detection of proteins in whole blood.* Electrochimica Acta, 2016. **212**: p. 1-9.

Bravo, K., et al., *Integrated bio-affinity nano-platform into a microfluidic immunosensor based on monoclonal bispecific trifunctional antibodies for the electrochemical determination of epithelial cancer biomarker.* Clinica Chimica Acta, 2017. **464**: p. 64-71.

Hiremath, N. and G. Bhat, *4 - High-performance carbon nanofibers and nanotubes*, in *Structure and Properties of High-Performance Fibers*. 2017, Woodhead Publishing: Oxford. p. 79-109.

Chung, D.D.L., *1 - Carbon Fibers, Nanofibers, and Nanotubes*, in *Carbon Composites (Second Edition)*. 2017, Butterworth-Heinemann. p. 1-87.

Hoffman, R.S. and M. Weinberg, *Use of human TNFα antibodies for treatment of erosive polyarthritis*. 2014, Google Patents.

Calero-Rubio, C., A. Saluja, and C.J. Roberts, *Coarse-Grained Antibody Models for "Weak" Protein–Protein Interactions from Low to High Concentrations.* The Journal of Physical Chemistry B, 2016. **120**(27): p. 6592-6605.

Cathou, R.E. and E. Haber, *Structure of the Antibody Combining Site. I. Hapten Stabilization of Antibody Conformation*.* Biochemistry, 1967. **6**(2): p. 513-518.

Shimba, N., N. Kamiya, and H. Nakamura, *Model Building of Antibody–Antigen Complex Structures Using GBSA Scores.* Journal of Chemical Information and Modeling, 2016. **56**(10): p. 2005-2012.

Zhao, X., et al., *Structural Insight of Antibody Adsorption for Improved Bioactivity and Detection*, in *Proteins at Interfaces III State of the Art*. 2012, American Chemical Society. p. 543-574.

Wolf, C. and Q. Li, *Tunable Two-Dimensional Array Patterning of Antibody Annuli through Microsphere Templating.* Langmuir, 2010. **26**(14): p. 12068-12074.

Kovář, M., et al., *Star Structure of Antibody-Targeted HPMA Copolymer-Bound Doxorubicin: A Novel Type of Polymeric Conjugate for Targeted Drug Delivery with Potent Antitumor Effect.* Bioconjugate Chemistry, 2002. **13**(2): p. 206-215.

Liu, Z., et al., *Radioimmunotherapy of Human Colon Cancer Xenografts with 131I-Labeled Anti-CEA Monoclonal Antibody.* Bioconjugate Chemistry, 2010. **21**(2): p. 314-318.

Li, C., et al., *Pancreatic Cancer Serum Detection Using a Lectin/Glyco-Antibody Array Method.* Journal of Proteome Research, 2009. **8**(2): p. 483-492.

Liu, S., et al., *Design, Synthesis, and Validation of Axl-Targeted Monoclonal Antibody Probe for microPET Imaging in Human Lung Cancer Xenograft.* Molecular Pharmaceutics, 2014. **11**(11): p. 3974-3979.

Hong, H., et al., *Multimodality Imaging of Breast Cancer Experimental Lung Metastasis with Bioluminescence and a Monoclonal Antibody Dual-Labeled with 89Zr and IRDye 800CW.* Molecular Pharmaceutics, 2012. **9**(8): p. 2339-2349.

Jin, H., et al., *Preclinical Evaluation of the Novel Monoclonal Antibody H6-11 for Prostate Cancer Imaging.* Molecular Pharmaceutics, 2013. **10**(10): p. 3655-3664.

Srinivasan, A.R., A. Lakshmikuttyamma, and S.A. Shoyele, *Investigation of the Stability and Cellular Uptake of Self-Associated Monoclonal Antibody (MAb) Nanoparticles by Non-Small Lung Cancer Cells.* Molecular Pharmaceutics, 2013. **10**(9): p. 3275-3284.

Mohsin, H., et al., *Radiolanthanide-Labeled Monoclonal Antibody CC49 for Radioimmunotherapy of Cancer: Biological Comparison of DOTA Conjugates and 149Pm, 166Ho, and 177Lu.* Bioconjugate Chemistry, 2006. **17**(2): p. 485-492.

Chen, J., et al., *Immuno Gold Nanocages with Tailored Optical Properties for Targeted Photothermal Destruction of Cancer Cells.* Nano Letters, 2007. **7**(5): p. 1318-1322.

Pu, C., et al., *Ultrasound-Mediated Destruction of LHRHa-Targeted and Paclitaxel-Loaded Lipid Microbubbles for the Treatment of Intraperitoneal Ovarian Cancer Xenografts.* Molecular Pharmaceutics, 2014. **11**(1): p. 49-58.

Su, Y., et al., *Gold Nanoparticles-Decorated Silicon Nanowires as Highly Efficient Near-Infrared Hyperthermia Agents for Cancer Cells Destruction.* Nano Letters, 2012. **12**(4): p. 1845-1850.

Yusupov, M., et al., *Plasma-Induced Destruction of Bacterial Cell Wall Components: A Reactive Molecular Dynamics Simulation.* The Journal of Physical Chemistry C, 2013. **117**(11): p. 5993-5998.

Peng, L.-H., et al., *Cell Membrane Capsules for Encapsulation of Chemotherapeutic and Cancer Cell Targeting in Vivo.* ACS Applied Materials & Interfaces, 2015. **7**(33): p. 18628-18637.

Hong, H., et al., *Generation and Screening of Monoclonal Antibodies for ImmunoPET Imaging of IGF1R in Prostate Cancer.* Molecular Pharmaceutics, 2014. **11**(10): p. 3624-3630.

Oldham, R.K. and R.O. Dillman, *Monoclonal Antibodies in Cancer Therapy: 25 Years of Progress.* Journal of Clinical Oncology, 2008. **26**(11): p. 1774-1777.

Junghans, R.P., et al., *Pharmacokinetics and Bioactivity of 1,4,7,10-tetra-azacylododecane N,N′,N″,N‴- tetraacetic acid (DOTA)-Bismuth-conjugated Anti-Tac Antibody for α-Emitter (²¹²Bi) Therapy.* Cancer Research, 1993. **53**(23): p. 5683-5689.

Bergmann-Leitner, E.S., et al., *Evaluation of immunoglobulin purification methods and their impact on quality and yield of antigen-specific antibodies.* Malaria Journal, 2008. **7**: p. 129-129.

Page, M. and R. Thorpe, *Purification of IgG Using DEAE-Sepharose Chromatography*, in *The Protein Protocols Handbook*, J.M. Walker, Editor. 2002, Humana Press: Totowa, NJ. p. 987-988.

Morais, V., P. Berasain, and H. Massaldi, *Immunoglobulin Purification by Caprylic Acid*, in *Protein Downstream Processing: Design, Development and Application of High and Low-Resolution Methods*, N.E. Labrou, Editor. 2014, Humana Press: Totowa, NJ. p. 137-143.

Harshman, J.S., *Purification of murine IgM monoclonal antibodies by hydroxylapatite chromatography.* Journal of tissue culture methods, 1989. **12**(3): p. 115-117.

Hall, R., P.D. Hunt, and R.G. Ridley, *Monoclonal Antibody Affinity Chromatography*, in *Protocols in Molecular Parasitology*, J.E. Hyde, Editor. 1993, Humana Press: Totowa, NJ. p. 389-395.

Suba, D., Z. Urbanyi, and A. Salgo, *Capillary isoelectric focusing method development and validation for investigation of recombinant therapeutic monoclonal antibody.* J Pharm Biomed Anal, 2015. **114**: p. 53-61.

Cao, J., et al., *Charge profiling and stability testing of biosimilar by capillary isoelectric focusing.* Electrophoresis, 2014. **35**(10): p. 1461-8.

Salas-Solano, O., et al., *Intercompany Study to Evaluate the Robustness of Capillary Isoelectric Focusing Technology for the Analysis of Monoclonal Antibodies.* Chromatographia, 2011. **73**(11-12): p. 1137-1144.

Zhou, C.M., *Characterization of human papillomavirus by capillary isoelectric focusing with whole-column imaging detection.* Electrophoresis, 2013. **34**(20-21): p. 3046-53.

Buszewski, B., E. Dziubakiewicz, and M. Szumski, *Electromigration techniques: theory and practice*. Vol. 105. 2013: Springer Science & Business Media.

Carlsson, M., et al., *Purification of in vitro produced mouse monoclonal antibodies. A two-step procedure utilizing cation exchange chromatography and gel filtration.* Journal of Immunological Methods, 1985. **79**(1): p. 89-98.

Cheng, X., et al., *Identification and separation of DNA-hybridized nanocolloids by Taylor cone harmonics.* Electrophoresis, 2009. **30**(18): p. 3236-41.

Lu, Y., et al., *Oxidative Post-Translational Modifications of an Amyloidogenic Immunoglobulin Light Chain Protein.* International Journal of Mass Spectrometry.

Mishra, L.N., N. Gupta, and S.M.R. Rao, *Mapping of post-translational modifications of spermatid-specific linker histone H1-like protein, HILS1.* Journal of Proteomics, 2015. **128**: p. 218-230.

Prabhu, L., et al., *Role of post-translational modification of the Y box binding protein 1 in human cancers.* Genes & Diseases, 2015. **2**(3): p. 240-246.

Zhang, Y., S.-L. Wu, and Y. Li, *Comparative study of profiling post-translational modifications of a circulating antibody drug in human with different capture reagents.* Biologicals.

Ma, Y., et al., *A multi-walled carbon nanotubes based molecularly imprinted polymers electrochemical sensor for the sensitive determination of HIV-p24.* Talanta, 2017. **164**: p. 121-127.

Arkan, E., et al., *A novel antibody–antigen based impedimetric immunosensor for low level detection of HER2 in serum samples of breast cancer patients via modification of a gold nanoparticles decorated multiwall carbon nanotube-ionic liquid electrode.* Analytica Chimica Acta, 2015. **874**: p. 66-74.

Zhu, X., et al., *Immunization with functionalized carbon nanotubes enhances the antibody response against mode antigen ovalbumin.* Immunology Letters, 2016. **178**: p. 77-84.

Hua, J., et al., *Preparation and properties of EDC/NHS mediated crosslinking poly (gamma-glutamic acid)/epsilon-polylysine hydrogels.* Materials Science and Engineering: C, 2016. **61**: p. 879-892.

Park, C., et al., *New method and characterization of self-assembled gelatin–oleic nanoparticles using a desolvation method via carbodiimide/N-hydroxysuccinimide (EDC/NHS) reaction.* European Journal of Pharmaceutics and Biopharmaceutics, 2015. **89**: p. 365-373.

Zhang, Y., et al., *Separation of monoclonal antibody charge state variants by open tubular capillary electrochromatography with immobilised protein as stationary phase*. Journal of Chromatography A, 2016. **1466**: p. 180-188.

Ghose, S., et al., *Modeling on-column reduction of trisulfide bonds in monoclonal antibodies during Protein A chromatography.* Journal of Chromatography A.

Formisano, N., et al., *Optimisation of an electrochemical impedance spectroscopy aptasensor by exploiting quartz crystal microbalance with dissipation signals.* Sensors and Actuators B: Chemical, 2015. **220**: p. 369-375.

Seo, H.W., S. Sarker, and D.M. Kim, *Electrochemical impedance spectroscopy of dye-sensitized solar cells with post-treated TiO2 photoelectrodes using hafnium(IV) chloride and titanium(IV) chloride.* Journal of Photochemistry and Photobiology A: Chemistry, 2017. **332**: p. 258-264.

Hazarika, J. and A. Kumar, *Studies of structural, optical, dielectric relaxation and ac conductivity of different alkylbenzenesulfonic acids doped polypyrrole nanofibers.* Physica B: Condensed Matter, 2016. **481**: p. 268-279.

Rusinek, C.A., et al., *Fabrication and characterization of boron doped diamond microelectrode arrays of varied geometry.* Electrochemistry Communications, 2016. **73**: p. 10-14.

Wightman, R.M., *Detection technologies. Probing cellular chemistry in biological systems with microelectrodes.* Science, 2006. **311**(5767): p. 1570-4.

Cahill, P.S., et al., *Microelectrodes for the measurement of catecholamines in biological systems.* Anal Chem, 1996. **68**(18): p. 3180-6.

Mecker, L.C., L.A. Filla, and R.S. Martin, *Use of a Carbon-ink Microelectrode Array for Signal Enhancement in Microchip Electrophoresis with Electrochemical Detection.* Electroanalysis, 2010. **22**(19): p. 2141-2146.

Larkin, P., *Chapter 3 - Instrumentation and Sampling Methods*, in *Infrared and Raman Spectroscopy*. 2011, Elsevier: Oxford. p. 27-54.

Larkin, P., *Chapter 1 - Introduction: Infrared and Raman Spectroscopy*, in *Infrared and Raman Spectroscopy*. 2011, Elsevier: Oxford. p. 1-5.

Larkin, P., *Chapter 8 - Illustrated IR and Raman Spectra Demonstrating Important Functional Groups*, in *Infrared and Raman Spectroscopy*. 2011, Elsevier: Oxford. p. 135-176.

Larkin, P., *Chapter 6 - IR and Raman Spectra-Structure Correlations: Characteristic Group Frequencies*, in *Infrared and Raman Spectroscopy*. 2011, Elsevier: Oxford. p. 73-115.

Fu, Y.Q., et al., *Recent developments on ZnO films for acoustic wave based bio-sensing and microfluidic applications: a review.* Sensors and Actuators B: Chemical, 2010. **143**(2): p. 606-619.

Peng, F., et al., *Bio-inspired design: Inner-motile multifunctional ZnO/CdS heterostructures magnetically actuated artificial cilia film for photocatalytic hydrogen evolution.* Applied Catalysis B: Environmental, 2015. **165**: p. 419-427.

Sang, C.-H., et al., *Fluorescence enhancement and multiple protein detection in ZnO nanostructure microfluidic devices.* Biosensors and Bioelectronics, 2016. **75**: p. 285-292.

APPENDIX 1

NYQUIS PLOTS

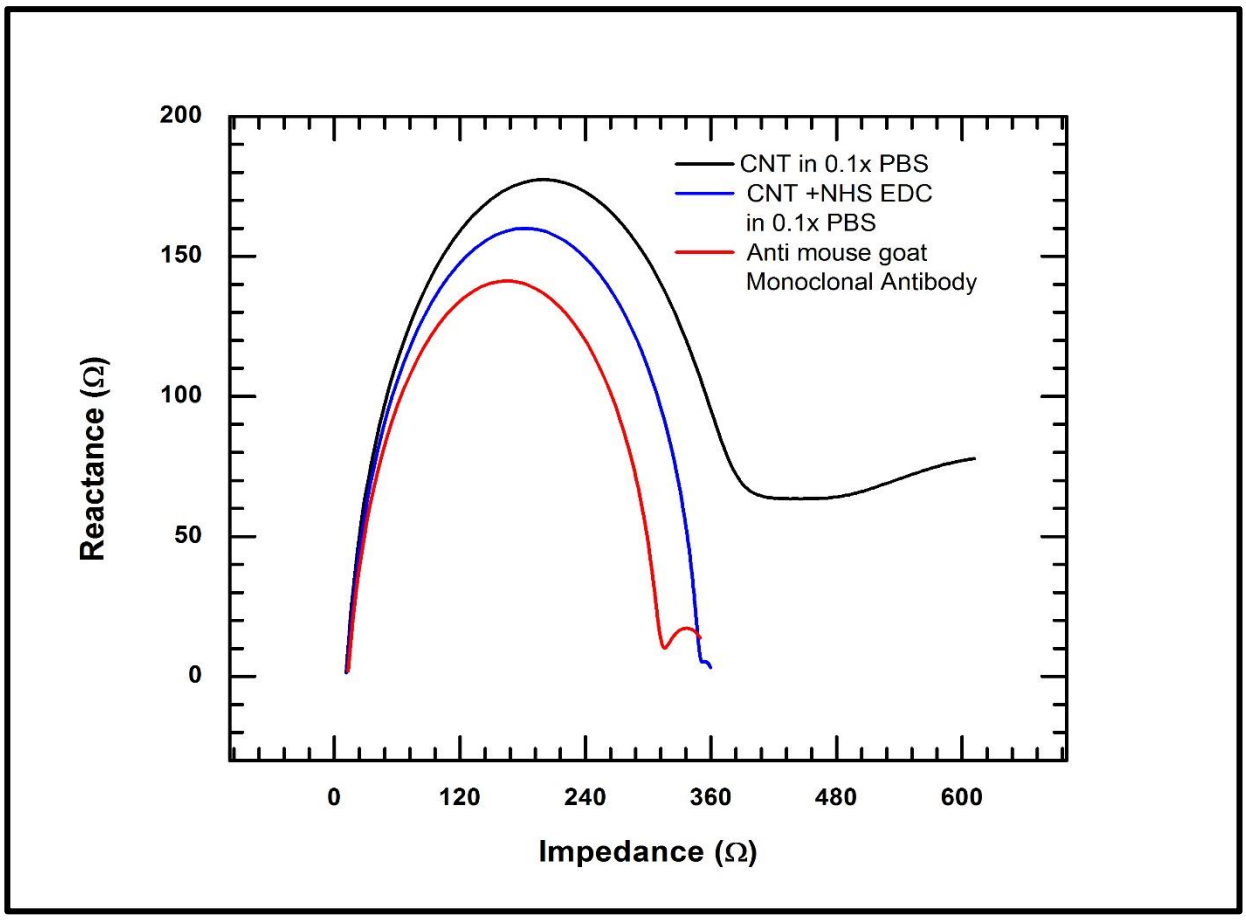

Figure A.1 A schematic illustration of impedance spectra in the form of Nyquist plots for a) Carbon Nanotube in 0.1x PBS, whose impedance is controlled by the diffusion to the and from the electrode surface (in black) b) Surface activation by EDC-NHS exhibiting a significant rise in impedance accompanied by a pronounced Warburg (in blue) c) Attachment of Anti Oxycodone mouse monoclonal antibody to functionalized CNTs (in red)

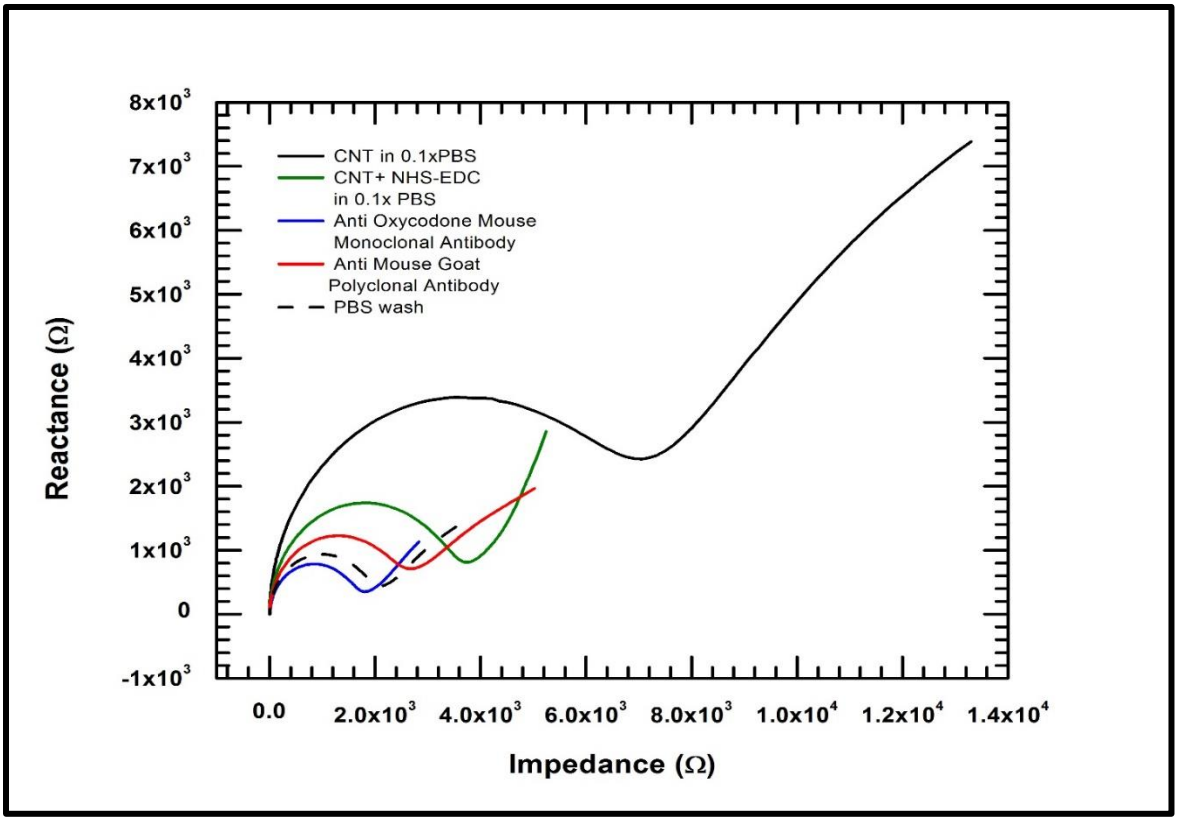

Figure A.2 A schematic illustration of impedance spectra in the form of Nyquist plots for a) Carbon Nanotube in 0.1x PBS, whose impedance is controlled by the diffusion to the and from the electrode surface (in black) b) Surface activation by EDC-NHS exhibiting a significant decrease in impedance accompanied by a pronounced Warburg (in green) c) Attachment of Anti Oxycodone mouse monoclonal antibody to functionalized CNTs (in blue) with further shift in impedance and Warburg d) Attachment of Anti-mouse goat polyclonal antibody to monoclonal antibody with significant change in impedance and Warburg (in red). e) PBS wash after 160 minutes that approximates the plot for monoclonal antibody attachment to functionalized CNTs (dotted lines).

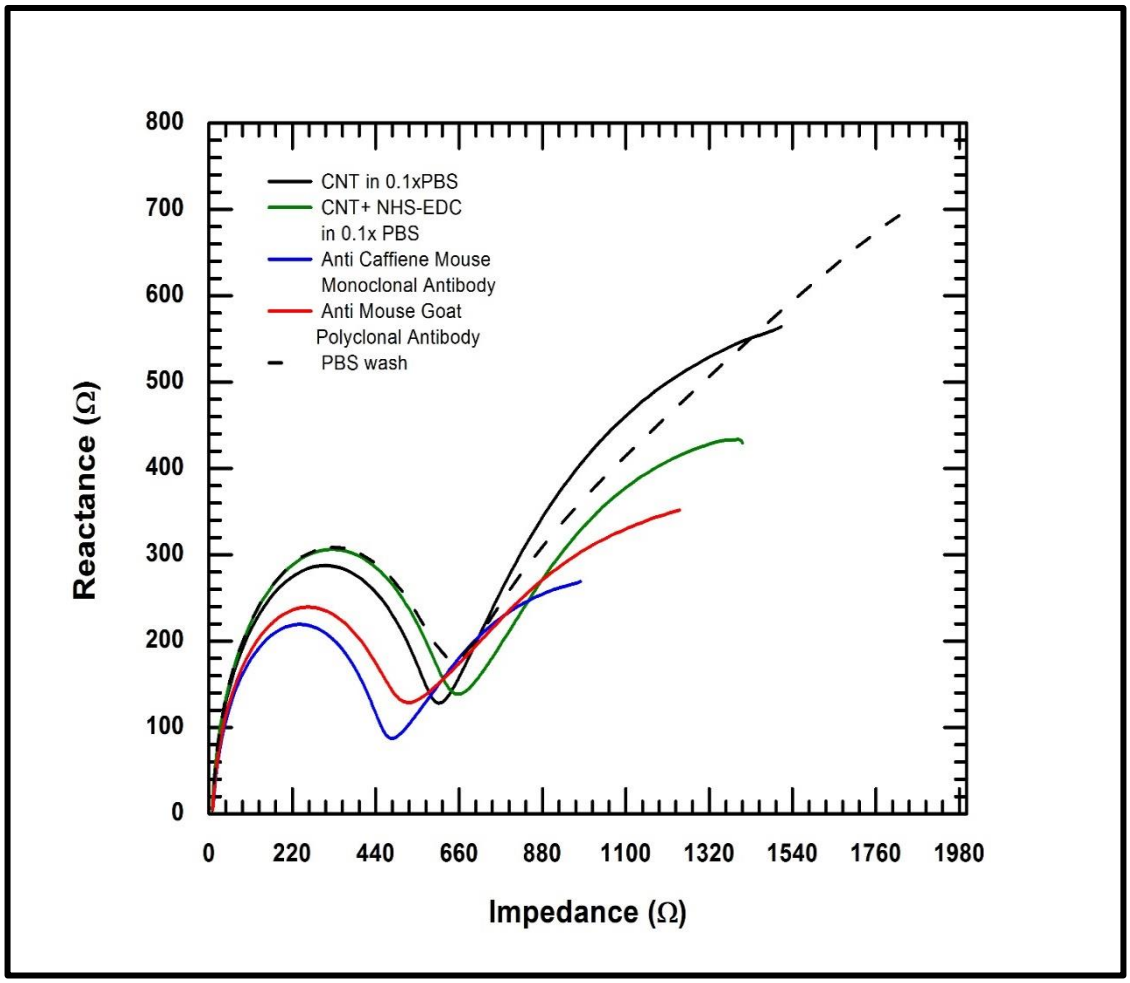

Figure: A.3 schematic illustration of impedance spectra in the form of Nyquist plots for a) Carbon Nanotube in 0.1x PBS, whose impedance is controlled by the diffusion to the and from the electrode surface (in black) b) Surface activation by EDC-NHS exhibiting a significant rise in impedance accompanied by a pronounced Warburg (in blue) c) Attachment of Anti Oxycodone mouse monoclonal antibody to functionalized CNTs (in green) with further shift in impedance and Warburg d) Attachment of Anti-mouse goat polyclonal antibody to monoclonal antibody with significant change in impedance and Warburg (in red). e) PBS wash after 160 minutes that approximates the plot for monoclonal antibody attachment to functionalized CNTs.

APPENDIX 2

BODE PLOT

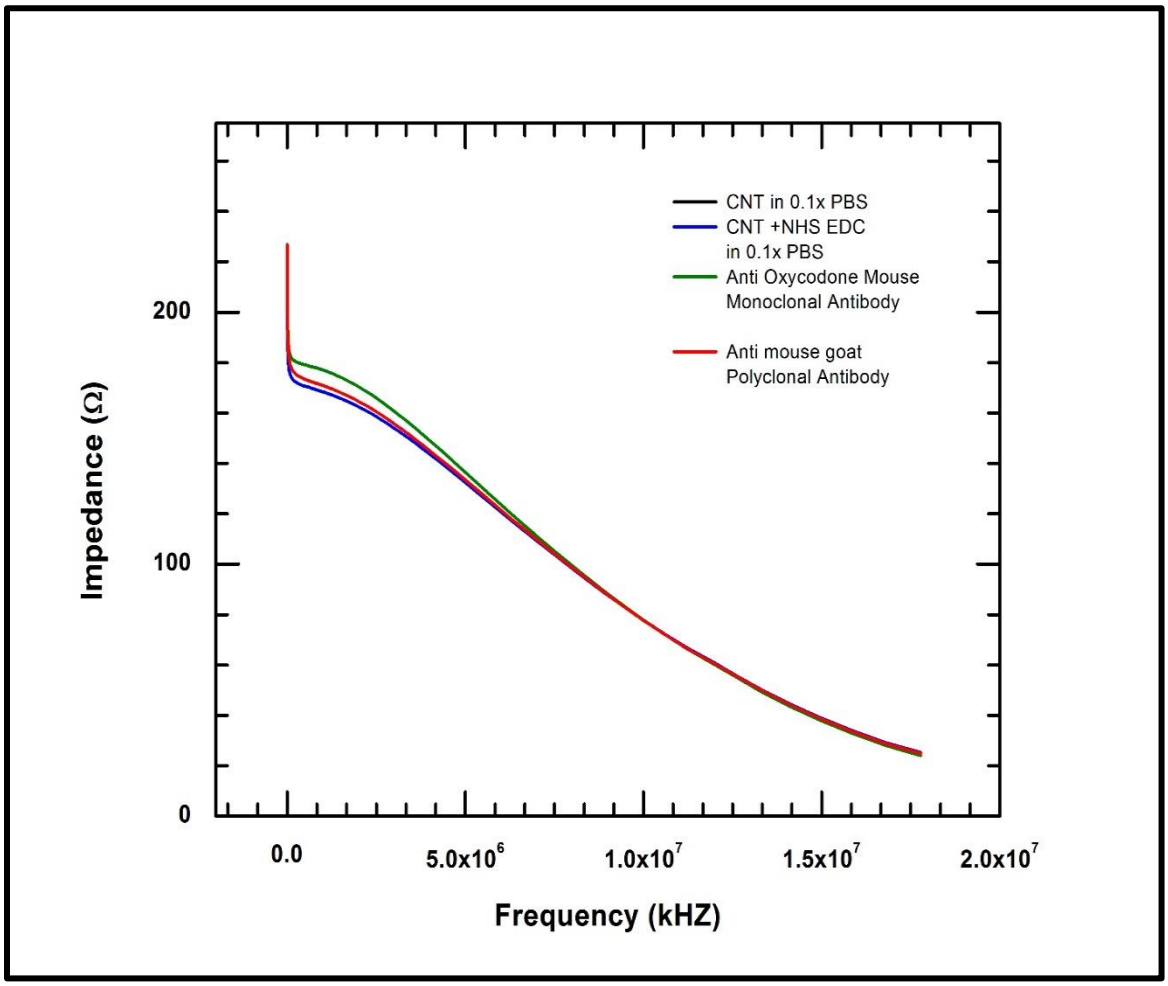

Figure A.4 A schematic illustration of the Bode plot for the batch process showing the impedance spectra the along the frequency domain. a) Carbon Nanotube in 0.1x PBS, (in black) b) Surface activation by EDC-NHS c) Attachment of Anti Oxycodone mouse monoclonal antibody to functionalized CNTs (in green) d) Attachment of Anti-mouse goat polyclonal antibody to monoclonal antibody (in red).

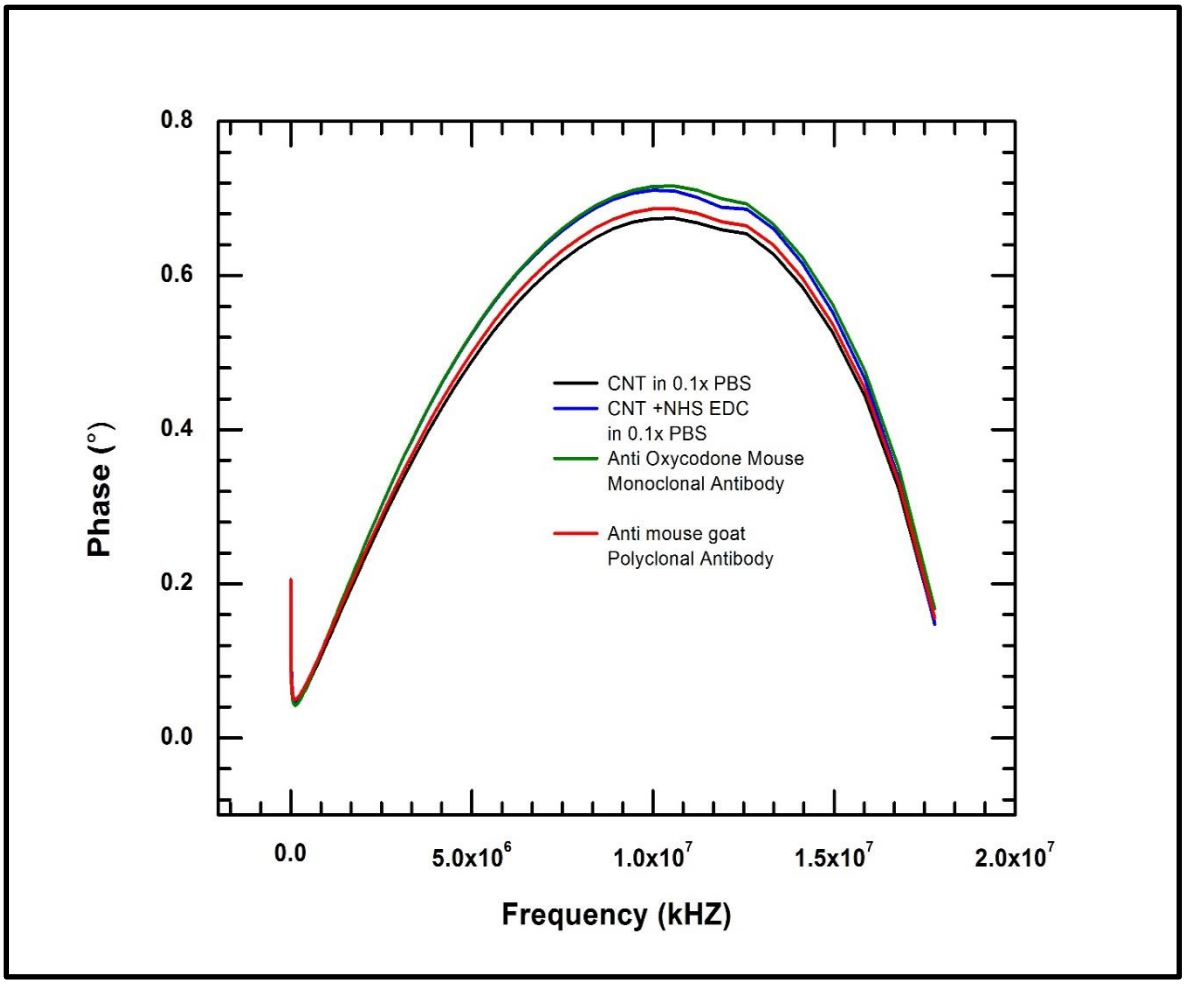

Figure A.5 A schematic illustration of the Bode plot for the batch process showing the phase spectra the along the frequency domain. a) Carbon Nanotube in 0.1x PBS, (in black) b) Surface activation by EDC-NHS c) Attachment of Anti Oxycodone mouse monoclonal antibody to functionalized CNTs (in green) d) Attachment of Anti-mouse goat polyclonal antibody to monoclonal antibody (in red).

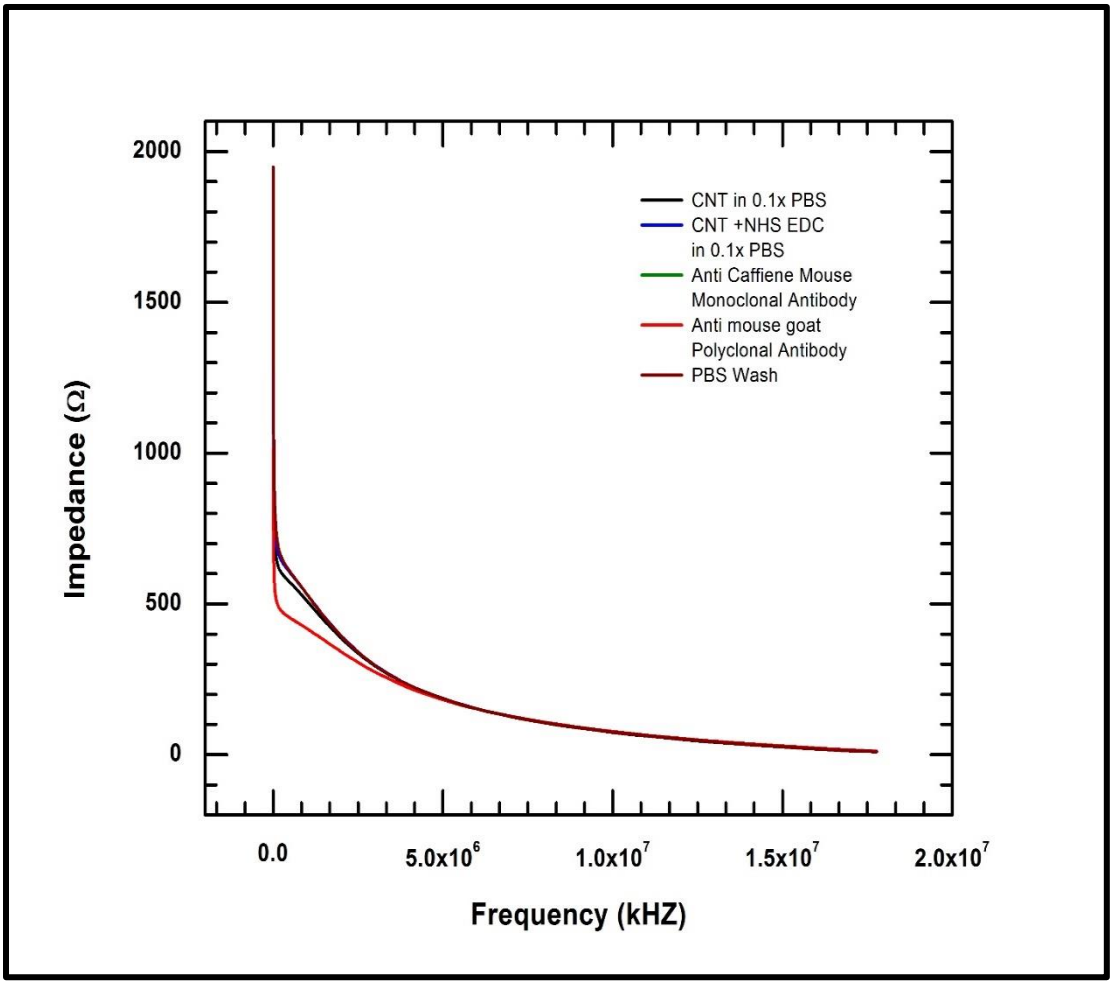

Figure A.6 A schematic illustration of the Bode plot for the batch process showing the impedance spectra the along the frequency domain. a) Carbon Nanotube in 0.1x PBS, (in black) b) Surface activation by EDC-NHS c) Attachment of Anti Caffierne mouse monoclonal antibody to functionalized CNTs (in green) d) Attachment of Anti-mouse goat polyclonal antibody to monoclonal antibody (in red).). e) PBS wash after 160 minutes that approximates the plot for monoclonal antibody attachment to functionalized CNTs.

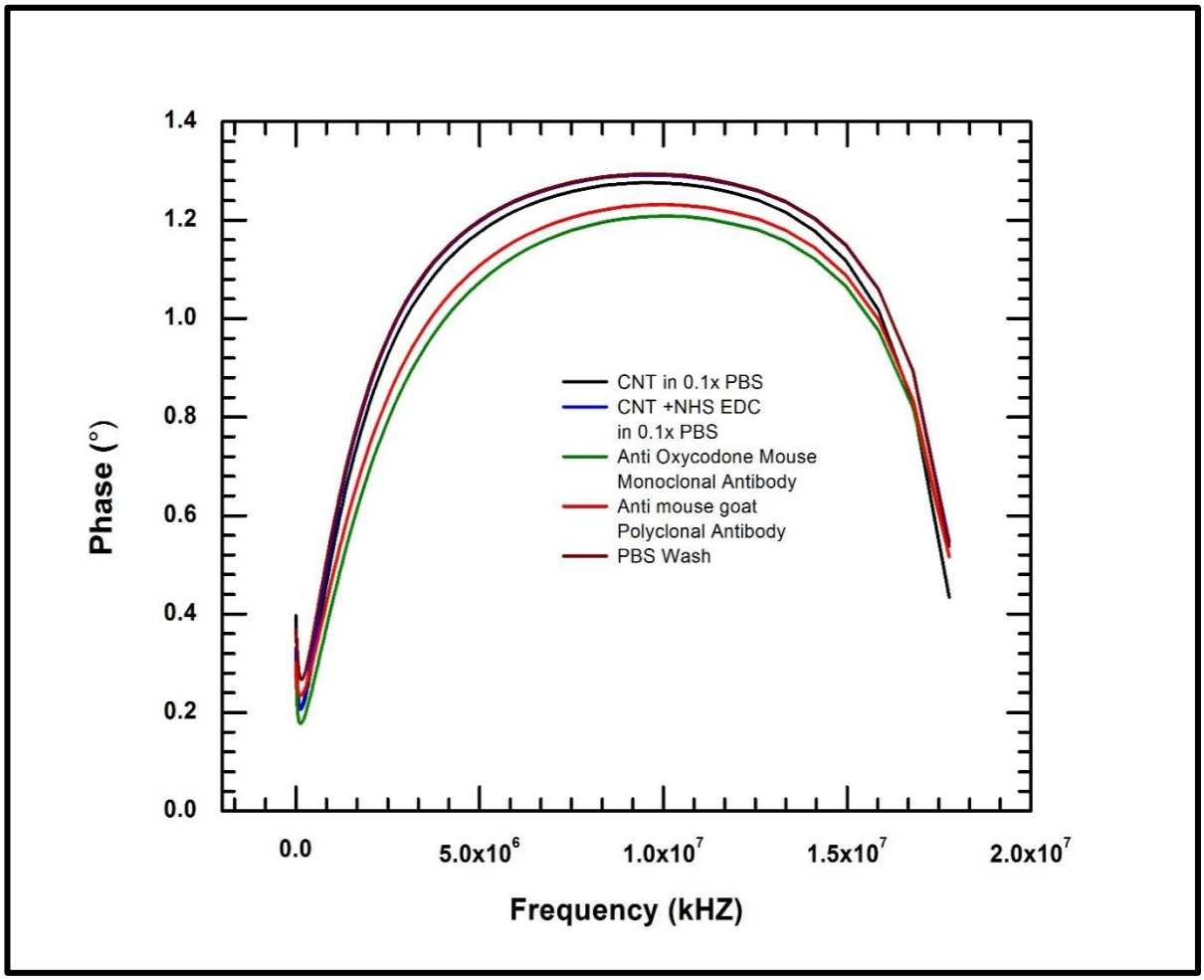

Figure A.7 A schematic illustration of the Bode plot for the batch process showing the phase spectra the along the frequency domain. a) Carbon Nanotube in 0.1x PBS, (in black) b) Surface activation by EDC-NHS c) Attachment of Anti Caffiene mouse monoclonal antibody to functionalized CNTs (in green) d) Attachment of Anti-mouse goat polyclonal antibody to monoclonal antibody (in red).). e) PBS wash after 160 minutes that approximates the plot for monoclonal antibody attachment to functionalized CNTs.

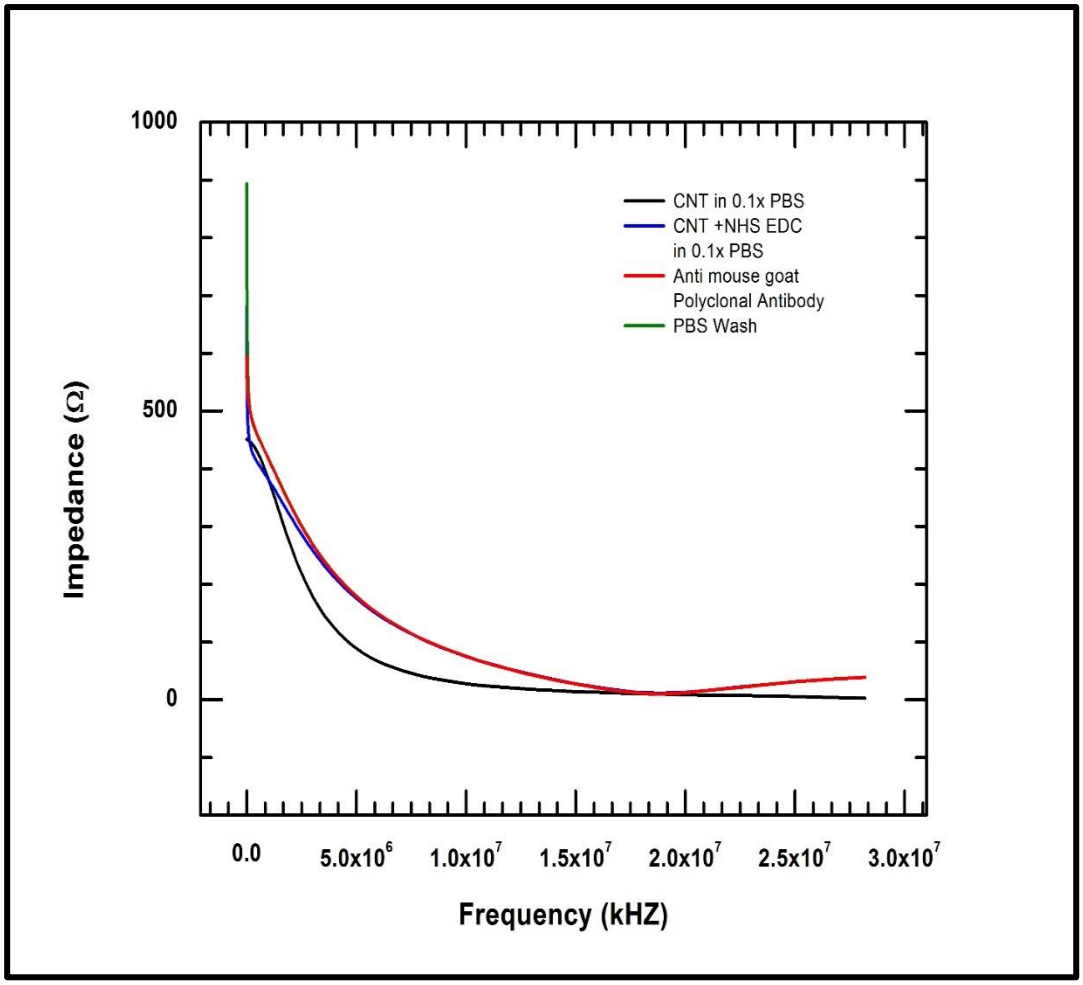

Figure A.8 A schematic illustration of the Bode plot for the batch process showing the phase spectra the along the frequency domain. a) Carbon Nanotube in 0.1x PBS, (in black) b) Surface activation by EDC-NHS c) Attachment of Anti-mouse goat polyclonal antibody to monoclonal antibody (in red).). e) PBS wash after 160 minutes that approximates the plot for monoclonal antibody attachment to functionalized CNTs (in green).